

Single-shot error correction of three-dimensional homological product codes

Armanda O. Quintavalle,^{1,*} Michael Vasmer,^{2,3,†} Joschka Roffe,^{1,‡} and Earl T. Campbell^{1,4,§}

¹*Department of Physics & Astronomy, University of Sheffield, Sheffield, S3 7RH, United Kingdom*

²*Perimeter Institute for Theoretical Physics, Waterloo, ON N2L 2Y5, Canada*

³*Institute for Quantum Computing, University of Waterloo, Waterloo, ON N2L 3G1, Canada*

⁴*AWS Center for Quantum Computing, Pasadena, CA 91125 USA*

Single-shot error correction corrects data noise using only a single round of noisy measurements on the data qubits, removing the need for intensive measurement repetition. We introduce a general concept of confinement for quantum codes, which roughly stipulates qubit errors cannot grow without triggering more measurement syndromes. We prove confinement is sufficient for single-shot decoding of adversarial errors. Further to this, we prove that all three-dimensional homological product codes exhibit confinement in their X -components and are therefore single-shot for adversarial phase-flip noise. For stochastic phase-flip noise, we numerically explore these codes and again find evidence of single-shot protection. Our Monte-Carlo simulations indicate sustainable thresholds of 3.08(4)% and 2.90(2)% for 3D surface and toric codes respectively, the highest observed single-shot thresholds to date. To demonstrate single-shot error correction beyond the class of topological codes, we also run simulations on a randomly constructed 3D homological product code.

I. INTRODUCTION

Quantum error correction encodes logical quantum information into a codespace [1]. Given perfect measurement of the codespace stabilisers we obtain the syndrome of any error present. A suitable decoding algorithm can determine a recovery operation that returns the system to the codespace. Either this recovery is a perfect success, or a failure resulting in a high weight logical error. However, in real quantum systems the measurements are not perfect and this simple story becomes more involved. The three main strategies for tackling noisy measurements are: repeated measurements on the code [2, 3]; performing measurement driven error-correction on a cluster state [4–9]; or using a single-shot code and decoder [10]. Focusing on the last strategy, the single-shot approach has the advantage of no additional time cost or cluster-state generation cost and provides a resilience against time-correlated noise [11]. In single-shot error correction, some residual error persists after each round of error correction, but this residual error is kept small and does not rapidly accumulate. However, only a special class of codes support single-shot error correction, but exactly which codes and why is not yet fully understood.

Bombín coined the phrase single-shot error correction and remarked that it “*is related to self-correction and confinement phenomena in the corresponding quantum Hamiltonian model.*” [10]. He defined confinement for subsystem codes, and showed that it is sufficient for single-shot error correction with a limited class of subsystem codes. In particular, he proved that the 3D gauge color code supports single-shot error correction, though it is unknown whether the corresponding Hamiltonian exhibits self-correction. Later single-shot error correction was numerically observed in a variety of higher dimensional topological codes, including: the

3D gauge color code [12], 4D surface codes [13] and their hyperbolic cousins [14], and 3D surface codes with phase noise [15–17]. Campbell established a general set of sufficient conditions, encapsulated by a code property called good soundness, that ensured adversarial noise [18] could be suppressed using a single-shot decoder. While Campbell’s sufficiency conditions explained single-shot error correction in a wide range of codes, around the same time it was shown that quantum expander codes [19–21] supported single-shot error correction [22]. However, quantum expander codes lack the soundness property so neither Bombín’s notion of confinement or Campbell’s notion of soundness is sufficient to encompass all known examples of single-shot error correction.

We can use different classical algorithms to decode a given quantum code, and this choice will affect the utility of the code. Different decoders have various time complexities and error tolerances, which affects the resources required by a quantum computer based on the code [23–25]. Thus far, single-shot decoders come in two flavours. The first are two-stage decoders [12, 13], where: stage 1 decoding repairs the noisy syndrome using redundancy in the parity check measurements; stage 2 decoding solves the corrected syndrome problem. The second flavour of decoders compute a correction from the noisy syndrome without attempting to repair it. Most examples of such decoders are local decoders, meaning that the whole correction is made up of corrections computed in small local regions of the code using syndrome information in the immediate neighbourhood [14–17, 21, 26, 27]. However, there are some examples of non-local decoders such as belief propagation (BP) being used for single-shot error correction without syndrome repair [14, 27]. A natural question to ask is: what is the optimal decoding strategy for single-shot codes? Even in the simple case of the 3D toric code this is not well-understood.

The remainder of this article is structured as follows. In Section II, we give a summary of our results. In Section III, we detail the construction of 3D product codes. In Section IV, we formally state our results on confinement and single-shot decoding in the adversarial noise setting. In Section V, we detail our numerical simulations and analyse their results. Fi-

* armandaoq@gmail.com

† mvasmer@perimeterinstitute.ca

‡ joschka@roffe.eu

§ earlrcampbell@gmail.com

nally, in Section VI, we discuss future research directions that flow from this work.

II. SUMMARY OF RESULTS

In this article, we investigate single-shot error correction of the class of 3D homological product codes [19, 28, 29], which we call 3D product codes. We review the construction of these codes in Section III, and show that the 3D surface and toric codes are particular instances of this more general class of codes in Appendix A. In Section IV, we introduce a general notion of confinement, which roughly stipulates that low-weight qubit errors will result in low-weight syndromes. We formalize the notion of a code family having good confinement, which we prove is a sufficient condition for single-shot decoding in the adversarial noise setting. We prove that all 3D product codes have confinement for phase-flip errors, and therefore have single-shot error correction for adversarial phase-flip noise. Furthermore, we expect these codes to have single-shot error correction for locally stochastic phase-flip noise as well. In fact, our definition of confinement generalises the definition proposed by Bombín [10] for the gauge color code and the notion of robustness for expander codes [20]; since both class of codes are proven to have a single-shot threshold for stochastic noise [10, 22] we conjecture that low density parity check (LDPC) codes with good confinement have a threshold too. We investigate this case numerically.

In the single-shot setting, the code always has some residual error present and the error correction procedure introduces noise correlations in subsequent rounds of single-shot error correction. How then do we assess success or failure? The concept of the sustainable threshold was proposed by Brown, Nickerson and Browne [12] as a metric for single-shot codes and decoders. We use $p_{\text{th}}(N)$ to denote the threshold of a code-decoder family given N cycles of qubit noise, noisy syndrome extraction and single-shot decoding, with the N^{th} cycle followed by a single round of noiseless syndrome extraction and decoding. The final round ensures that we can return the system to the codespace and assess success by the absence of a logical error. We define the sustainable threshold of the code-decoder family to be

$$p_{\text{sus}} = \lim_{N \rightarrow \infty} p_{\text{th}}(N). \quad (1)$$

Numerically, this is estimated by plotting $p_{\text{th}}(N)$ against N and fitting to the following ansatz,

$$p_{\text{th}}(N) = p_{\text{sus}}[1 - (1 - p_{\text{th}}(0)/p_{\text{sus}})e^{-\gamma N}]. \quad (2)$$

We numerically estimate the sustainable error thresholds of 3D toric and surface codes for two different two-stage decoders. We surpass all previous single-shot error thresholds for these code families, and we also obtain the highest code-capacity noise (no measurement error) threshold; see Table I. For our single-shot simulations, we use an independent and identically distributed (iid) noise model where each qubit experiences a phase-flip error with probability p , and

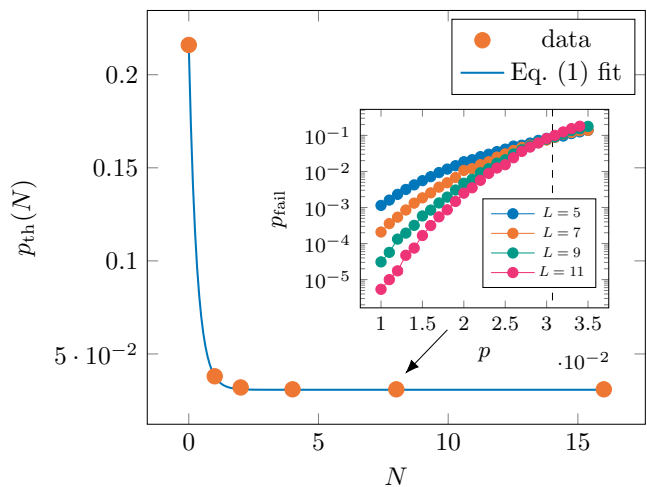


FIG. 1. Numerical estimate of the sustainable threshold of the 3D surface code for a two-stage decoder where we repair the syndrome using MWPM, and solve the corrected syndrome problem using BP+OSD. We plot the error threshold $p_{\text{th}}(N)$ for different numbers of cycles, N . Using the ansatz in Eq. (2), we estimate the sustainable threshold to be $p_{\text{sus}} = 0.0308(4)$ with $\gamma = 3.23$. The inset shows a plot of the logical error rate, p_{fail} , against the phase-flip and measurement error rate, p , for $N = 8$. The error threshold $p_{\text{th}}(8)$ is the point at which the curves intersect (L is the code distance).

each stabiliser measurement outcome is flipped with probability $q = p$. We investigate two decoding strategies: one where we use minimum-weight perfect matching (MWPM) for stage 1 decoding and belief propagation with ordered statistics decoding (BP+OSD) for stage 2 decoding and another where we use BP+OSD for both decoding stages. Figure 1 shows the 3D surface code sustainable threshold fit, using the MWPM & BP+OSD decoding strategy. We find a comparable sustainable threshold for the 3D surface code using BP+OSD for both decoding stages, as shown in Table II. We achieve very similar performance for the 3D toric code, although there is a subtlety present in stage 1 decoding that is not present in the 3D surface code case; see Section V C. For both code families, we provide evidence that the performance of stage 1 decoding is the bottleneck of the full decoding procedure, and we achieve near-optimal performance within this constraint.

Decoder	$q = 0$	$q = p$
Erasure Mapping [30]	12.2%	N/A
Toom's Rule [15]	14.5%	N/A
Sweep* [17]	15.5%	1.7%
Renormalization Group [13]	17.2%	7.3(1)%
Neural Network [31]	17.5%	7.1(3)%
MWPM + BP/OSD*	21.55(1)%	2.90(2)%
Optimal [32–36]	23.180(4)%	11.0%

TABLE I. Comparison of the error thresholds of toric code decoders against phase-flip noise with ($q = p$) and without ($q = 0$) measurement errors. Starred entries are single-shot decoders. Unstarred entries use the whole syndrome history. Text in bold highlights our results.

Code	MWPM & BP+OSD	BP+OSD x2
Surface	3.08(4)%	2.90(1)%
Toric	2.90(2)%	2.78(2)%

TABLE II. Sustainable thresholds for 3D toric and surface codes for different single-shot decoding strategies. For each entry in the table, we did an analogous simulation to that described in Fig. 1. The numbers in brackets are the standard errors.

The advantage of using BP+OSD for stage 1 decoding is that, unlike MWPM, this decoder does not rely on the special structure of the loop-like syndrome present in 3D toric and surface codes. Therefore, we anticipate that one can use BP+OSD for single-shot decoding of general 3D product codes. We numerically test this prediction by decoding a family of non-topological 3D product codes using BP+OSD for both decoding stages, achieving sustainable thresholds that are comparable to those of the 3D toric and surface codes. This provides evidence that BP+OSD can be used as a generic two-stage decoder for single-shot LDPC 3D product codes.

III. CODE CONSTRUCTION

A stabiliser code encoding k logical qubits into n physical qubits can be described by its stabiliser group \mathcal{S} and a syndrome map $\sigma(\cdot)$. The stabiliser group \mathcal{S} is an Abelian subgroup of the Pauli group \mathcal{P}_n on n qubits which does not contain $-\mathbb{1}$ and has dimension $n - k$. The syndrome map is not unique: any generating set of the group \mathcal{S} defines a valid syndrome map for the code. If $\{S_1, \dots, S_m\}$ is one of such generating sets, the associate function $\sigma(\cdot)$ maps a qubit operator $P \in \mathcal{P}_n$ into the binary vector $(s_1, \dots, s_m)^T \in \mathbb{F}_2^m$, where $s_i = 1$ if S_i anti-commutes with P and 0 otherwise. Importantly, $\sigma(\cdot)$ is linear, meaning that $\sigma(P \cdot Q) = \sigma(P) + \sigma(Q)$ over \mathbb{F}_2^m . Moreover, because any Pauli operator can be factorised as the product of an X and a Z -operator P_X and P_Z , we can identify any $P \in \mathcal{P}_n$ with a binary vector $v = (v_X, v_Z)^T$ in \mathbb{F}_2^{2n} , where the i th entry of v_X/v_Z is 1 if and only if P_X/P_Z acts non-trivially on the i th qubit. This identification is a group homomorphism (i.e. multiplication of Pauli operators corresponds to the sum of their vector representation in \mathbb{F}_2^{2n}) and since $\sigma(\cdot)$ is linear, syndrome measurement can be simulated via a matrix-vector product:

$$\sigma : \mathbb{F}_2^{2n} \longrightarrow \mathbb{F}_2^m$$

$$\begin{pmatrix} v_X \\ v_Z \end{pmatrix} \mapsto H \begin{pmatrix} v_X \\ v_Z \end{pmatrix}$$

where the vector $(v_X, v_Z)^T \in \mathbb{F}_2^{2n}$ represents a Pauli error on the physical qubits. Following the nomenclature from classical coding theory, we refer to syndrome matrix H as parity check matrix and we say that a code is LDPC when its parity check is low density.

The weight $|\cdot|$ of a Pauli operator $P \in \mathcal{P}_n$ is the number of qubits on which its action is different from the identity. A stabiliser code is said to be distance d if d is the minimum weight of a Pauli operator not in \mathcal{S} that has trivial syndrome.

We will refer to a code of length n , dimension k and distance d as a $[[n, k, d]]$ code.

A stabiliser code is a CSS code if its stabiliser group can be generated by the disjoint union of a set of X -operators and a set of Z -operators. In this case, its parity check is a block matrix:

$$H = \left(\begin{array}{c|c} 0 & H_X \\ \hline H_Z & 0 \end{array} \right) \quad (3)$$

where H_X has size $m_x \times n$ and H_Z has size $m_z \times n$ if the generating set of X -stabilisers/ Z -stabilisers has cardinality m_x/m_z . Eq. (3) entails that syndrome extraction can be performed separately for the X -component and for the Z -component. In fact, if a Pauli operator has vector representation $(v_X, v_Z)^T = (v_X, 0)^T + (0, v_Z)^T \in \mathbb{F}_2^{2n}$, then for its syndrome holds:

$$\begin{aligned} H \begin{pmatrix} v_X \\ v_Z \end{pmatrix} &= H \begin{pmatrix} v_X \\ 0 \end{pmatrix} + H \begin{pmatrix} 0 \\ v_Z \end{pmatrix} \\ &= \begin{pmatrix} 0 \\ H_Z v_Z \end{pmatrix} + \begin{pmatrix} H_X v_X \\ 0 \end{pmatrix} \\ &= \begin{pmatrix} 0 \\ s_Z \end{pmatrix} + \begin{pmatrix} s_X \\ 0 \end{pmatrix} \end{aligned}$$

where $s_Z \in \mathbb{F}_2^{m_z}$ and $s_X \in \mathbb{F}_2^{m_x}$. In other words, it is possible to truncate these vectors without losing information and deal with X and Z operators separately. For this reason, we say that a CSS code is provided with two syndrome maps which correspond to the two blocks/matrices H_X and H_Z respectively. Accordingly, a CSS code will have a Z -distance and a X -distance and can be compactly be referred to as a $[[n, k, d_x, d_z]]$ code.

To our purpose, it is handy to describe CSS codes in terms of chain complexes. A chain complex of length ℓ is a collection of vector spaces C^0, \dots, C^ℓ and linear maps $\delta_i : C^i \rightarrow C^{i+1}$ with the only constraint

$$\delta_{i+1} \delta_i = 0, \quad (4)$$

for $i = 0, \dots, \ell - 1$. If H_X and H_Z are $m_x \times n$ and $m_z \times n$ binary matrices as in Eq. (3), then the chain complex:

$$\mathbb{F}_2^{m_z} \xrightarrow{H_Z^T} \mathbb{F}_2^n \xrightarrow{H_X} \mathbb{F}_2^{m_x} \quad (5)$$

is well defined. In fact, the commutative condition on the stabilisers of the code entails that the X -generators and the Z -generators of the code have even overlap, such that they are orthogonal when seen as binary vectors. In other words, $H_X \cdot H_Z^T = 0$ is equivalent to the defining property of the chain complexes (see Eq. (4)). In general, we can associate a CSS code to any chain complex $\{C^i, \delta_i\}$ of length at least 3 by equating $H_Z^T = \delta_i$ and $H_X = \delta_{i+1}$ for some index i . In the chain complex language, we say that the code has length $\dim C_{i+1}$ and the dimension of the $(i+1)$ -th homology group $\mathcal{H}_{i+1} = \ker \delta_{i+1} / \text{Im } \delta_i$. Equivalently, the dimension of the code is the dimension of the $(i+1)$ -th cohomology group $\mathcal{H}_{i+1}^* = \ker \delta_i^T / \text{Im } \delta_{i+1}^T$. The X and Z distances are given

respectively by the minimum weight of any non-zero vector in \mathcal{H}_{i+1}^* and \mathcal{H}_{i+1} .

Here, we study some decoding properties of 3D product codes. By this nomenclature we refer to the CSS codes obtained by the homological product of three length-1 chain complexes as described in [37]. Given three classical linear codes with parity check matrices δ_A, δ_B and δ_C we can build a 3D quantum code as follows. If δ_ℓ is a binary matrix of size $m_\ell \times n_\ell$, it defines a linear map $\delta_\ell : C_\ell^0 \rightarrow C_\ell^1$, where C_ℓ^0, C_ℓ^1 are vector spaces over \mathbb{F}_2 of dimension n_ℓ and m_ℓ respectively; in other words, each linear map defines a length-1 chain complex. Their product is the length-3 chain complex \mathcal{C} given by:

where:

$$\delta_0 = \begin{pmatrix} \delta_A \otimes \mathbb{1} \otimes \mathbb{1} \\ \mathbb{1} \otimes \delta_B \otimes \mathbb{1} \\ \mathbb{1} \otimes \mathbb{1} \otimes \delta_C \end{pmatrix},$$

$$\delta_1 = \begin{pmatrix} \mathbb{1} \otimes \delta_B \otimes \mathbb{1} & \delta_A \otimes \mathbb{1} \otimes \mathbb{1} & 0 \\ \mathbb{1} \otimes \mathbb{1} \otimes \delta_C & 0 & \delta_A \otimes \mathbb{1} \otimes \mathbb{1} \\ 0 & \mathbb{1} \otimes \mathbb{1} \otimes \delta_C & \mathbb{1} \otimes \delta_B \otimes \mathbb{1} \end{pmatrix},$$

$$\delta_2 = (\mathbb{1} \otimes \mathbb{1} \otimes \delta_C \quad \mathbb{1} \otimes \delta_B \otimes \mathbb{1} \quad \delta_A \otimes \mathbb{1} \otimes \mathbb{1}).$$

Here, the symbol \otimes represents the tensor product. Given two vector spaces A and B over a field \mathbb{F} , their tensor product is the vector space $A \otimes B$ generated by the formal sums $\sum a \otimes b$ where $a \in A$ and $b \in B$ and the operator \otimes is bilinear, i.e. for any a_1, a_2, b_1, b_2 in A and B respectively, it holds that

$$(a_1 + a_2) \otimes b_1 = a_1 \otimes b_1 + a_2 \otimes b_1, \\ a_1 \otimes (b_1 + b_2) = a_1 \otimes b_1 + a_1 \otimes b_2.$$

The horizontal stacking of spaces, instead, represents their direct sum.

It is easy to verify that condition (4) is verified for $i = 1, \dots, 3$ and therefore the chain complex \mathcal{C} is well defined. As explained above, we define a CSS code on \mathcal{C} by equating

$$H_Z = \delta_0^T, \quad H_X = \delta_1.$$

We refer to the matrix $M = \delta_2$ as the metacheck matrix for the X -stabilisers. Condition (4) entails $MH_X = 0$ and as a consequence we can think of the matrix M as a parity

check matrix on the X syndromes: any valid X -syndrome satisfies the constraints defined by M . Suppose that the classical linear code with parity check matrix δ_ℓ has parameters $[n_\ell, k_\ell, \delta_\ell]$ and the code with parity check matrix δ_ℓ^T has parameters $[n_\ell^T, k_\ell^T, d_\ell^T]$, where, by convention, the distance of a code with dimension 0 is ∞ . Then, as showed in [37], \mathcal{C} is associated with an $[[n, k, d_x, d_z]]$ code where

$$n = n_a^T n_b n_c + n_a n_b^T n_c + n_a n_b n_c^T \\ k = k_a^T k_b k_c + k_a k_b^T k_c + k_a k_b k_c^T \\ d_x = \min\{d_b d_c, d_a d_c, d_a d_b\} \\ d_z = \min\{d_a^T, d_b^T, d_c^T\}$$

We define the single-shot distance d_{ss} [18] of the chain complex \mathcal{C} as the minimum weight of a vector in \mathcal{C}_2 that satisfies all the constraints given by δ_2 (i.e. it belongs to the kernel of δ_2) but is not a valid X -syndrome (i.e. it does not belong to the image of δ_1). In other words, d_{ss} is the minimum weight of a vector in the second homology group $\mathcal{H}_2 = \ker \delta_2 / \text{Im } \delta_1$ of the chain complex \mathcal{C} and following [37] it is easy to verify that $d_{ss} = \min\{d_a, d_b, d_c\}$.

It is important to note that, if the matrices δ_ℓ are LDPC, then the quantum code is LDPC too. In fact, if δ_ℓ has column (row) of weight bounded by c_ℓ (r_ℓ), then δ_i has column and row weight bounded by c_i and r_i respectively where:

- i. $c_0 \leq c_a + c_b + c_c$ and $r_0 \leq \max\{r_a, r_b, r_c\}$;
- ii. $c_1 \leq \max\{c_a + c_b, c_a + c_c, c_b + c_c\}$
and
 $r_1 \leq \max\{r_a + r_b, r_a + r_c, r_b + r_c\}$;
- iii. $c_2 \leq \max\{c_a, c_b, c_c\}$ and $r_2 \leq r_a + r_b + r_c$.

A. On geometric locality

Apart from preserving the LDPC properties of the seed matrices δ_A, δ_B and δ_C , the 3D homological product allows for the construction of codes with local interactions when qubits are placed on a 3D cubic lattice. We defer to App. A for a thorough discussion on this subject but here present a summary.

As explained above, qubits of a 3D product code associated to the chain complex \mathcal{C} are in bijection with basis elements of the space \mathcal{C}_1 ; since \mathcal{C}_1 is the direct sum of the three vector spaces $C_A^1 \otimes C_B^0 \otimes C_C^0$, $C_A^0 \otimes C_B^1 \otimes C_C^0$ and $C_A^0 \otimes C_B^0 \otimes C_C^1$ we introduce three different type of qubits: *transverse*, *vertical* and *horizontal*. Qubit types naturally correspond to the three different orientation of edges on the cubic lattice, namely edges parallel to each of the three crystal planes. Referring to this particular display of qubits, the stabilisers of the code defined by \mathcal{C} have support as follows:

1. X -stabilisers have support on a 2D cross of qubits of two types out of three, contained in one of the three crystal planes; the crossing is defined by a square face of a cube (see Fig. 5c);

2. Z -stabilisers have support on a 3D cross of qubits, with crossing defined by a vertex of a cube (see Fig. 5d).

The cubic lattice considered can present some irregularities: in general it is a cubic lattice with some missing edges (see App. A). Nonetheless, square faces and vertices are uniquely defined and they correspond to a stabiliser every time they contain at least one edge. More specifically, a square face identifies two perpendicular lines of edges/qubits on a plane (i.e. the edges parallel to the boundary of the square face itself): the corresponding X -stabiliser has support contained on those lines of qubits. Similarly, a vertex identifies three perpendicular lines of qubits and the corresponding Z -stabiliser has support there contained. This ‘cross shape’ of the stabilisers’ support, combined with some locality properties of the seed matrices, allows us to show (Prop. 1 in App. A 1) that 3D product codes are local on a 3D cubic lattice. Here, by locality, we mean:

1. any X -stabiliser generator has weight at most 2ρ with support contained in a 2D box of size $\rho \times \rho$,
2. any Z -stabiliser generator has weight at most 3ρ with support contained in a 3D box of size $\rho \times \rho \times \rho$,

for some positive integer ρ .

Interestingly, an explicit construction of the 3D toric and surface codes as 3D product codes follows easily as a corollary of our locality proof. We here report how to build the toric and the surface code as 3D product codes and we defer to App. A for further details.

The 3D toric code is the 3D product code obtained by choosing $\delta_A = \delta_B = \delta_C = \delta$ as seed matrices, where δ is the parity check matrix of the repetition code. For instance, the 3D toric code with linear lattice size $L = 3$ is given by

$$\delta = \begin{pmatrix} 1 & 1 & 0 \\ 0 & 1 & 1 \\ 1 & 0 & 1 \end{pmatrix}.$$

In general, the 3D toric code of lattice size L , has parameters

$$[[3L^3, 3, L^2, L]],$$

and single-shot distance $d_{ss} = L$.

The 3D surface code is obtained from this construction by choosing, for linear lattice size $L = 3$,

$$\delta_A = \delta_B = \begin{pmatrix} 1 & 1 & 0 \\ 0 & 1 & 1 \end{pmatrix}$$

and

$$\delta_C = \begin{pmatrix} 1 & 1 & 0 \\ 0 & 1 & 1 \end{pmatrix}^T$$

Therefore, for lattice size L , it has parameters

$$[[2L(L-1)^2 + L^3, 1, L^2, L]],$$

and single-shot distance $d_{ss} = \infty$.

Further details can be found in App. A.

B. Non-topological codes

The 3D product code construction can be used to obtain non-topological codes with non-local interactions. Table III shows the parameters for a class of non-topological codes based on classical LDPC codes. The specific advantage of non-topological codes is that it is possible to construct code families where the number logical qubits increases with code size. This is in contrast to 3D toric and surface codes, where the number of logical qubits is fixed for all values of the code distance.

δ_A	δ_B	δ_C	$\mathcal{HGP}(\delta_A, \delta_B, \delta_C)$
[16, 4, 6]	[6, 1, 6]	[6, 0, ∞]	[[1336, 4, 6]]
[20, 5, 8]	[8, 1, 8]	[8, 0, ∞]	[[3100, 5, 8]]
[24, 6, 10]	[10, 1, 10]	[10, 0, ∞]	[[5964, 6, 10]]

TABLE III. A family of 3D product codes. The base codes $\{\delta_A, \delta_B, \delta_C\}$ are set as follows: δ_A is a parity check matrix of an $[[n, k, d]]$ (3,4)-LDPC code; δ_B is a $[[L, 1, L]]$ repetition code; δ_C is the transpose of a $[[L, 1, L]]$ repetition code. The code distance is set to ∞ for codes of dimension 0.

IV. FORMAL STATEMENTS

In this Section, we introduce the definition of *confinement* for a stabiliser code and exhibit a theoretical two-stage decoder, the *Ball decoder*, which we prove to be single-shot in the adversarial setting for confined codes.

The concept of confinement is closely related to soundness [18] but it is weaker and so able to encompass more families of codes, such as the expander codes [19–21] which are confined but not sound. Roughly speaking, a code has good confinement if small qubit errors produce small measurement syndromes; this differs from good soundness which entails that small syndromes can be produced by small errors.

The Ball decoder differs from previous single-shot two stage decoders (e.g. the MW single-shot decoder introduced in Definition 6 of [18]) in that it does not rely on metachecks on syndromes. If syndromes are protected by a classical code, as it is the case for X -syndromes of 3D product codes introduced in Section III, then a single-shot decoding strategy could work as follows: (1) correct the measured syndrome whenever it does not satisfy all the constraints defined by the metacode; (2) find a recovery operator on qubits that has syndrome equal to the one found at point (1). The Ball decoder, instead, corrects the syndrome both anytime it fails to satisfy all the constraints of the metacode and when it is generated by high weight errors.

We remind the reader that given a Pauli operator P , its weight $|P|$ is the number of qubits on which its action is not the identity. Given a stabiliser code with stabiliser group \mathcal{S} , the reduced weight of a Pauli operator P on the physical qubits is

$$|P|_{\text{red}} = \min\{|PS| : S \in \mathcal{S}\} \quad (6)$$

For a stabiliser code, we then have

Definition 1 (Confinement). *Let t be an integer and $f : \mathbb{Z} \rightarrow \mathbb{Z}$ some increasing function with $f(0) = 0$. Given a stabiliser code we say it has (t, f) -confinement if for all errors E with $|E|_{\text{red}} \leq t$, it follows that $f(|\sigma(E)|) \geq |E|_{\text{red}}$.*

Let us contrast this with Bombín’s notion of confinement (Def. 16 of Ref. [10]) that has some similarities but only allows for linear functions of the form $f(x) = Kx$ for some constant K . Many codes, including 3D product codes, have superlinear confinement functions, and so Bombín’s definition does not encompass them.

We also define the following notion of good confinement for a family of stabiliser codes

Definition 2 (Good confinement). *Consider an infinite family of stabiliser codes. We say that the family has good confinement if each code in it has (t, f) -confinement where:*

1. t grows with the length n of the code: $t \in \Omega(n^b)$ with $b > 0$;
2. and $f(\cdot)$ is monotonically increasing and independent of n .

We say the code family has good X -confinement if the above holds only for Pauli- Z errors.

Our main analytic result is that codes with good confinement are single-shot

Theorem 1. *Consider a family of $[[n, k, d]]$ quantum-LDPC codes with good confinement such that $d \geq an^b$ with $a > 0$ and $b > 0$. This code family is single-shot for the adversarial noise model. If the code family only has good X -confinement then it is single-shot with respect to Pauli- Z noise.*

We further prove that 3D product codes have X -confinement:

Theorem 2. *All 3D product codes have (t, f) X -confinement where t is equal to the Z -distance of the code and $f(x) = \frac{x^3}{2}$ or better.*

These two results together motivates our numerical experiments reported in Sec. V. We conjecture that the result of Theorem 1 can be extended to deal with local stochastic noise and used to show that LDPC codes with good confinement have a single-shot threshold.

We now proceed to prove Theorem 1. To this end, we use the Ball decoder that we introduce in Definition 3. We do not describe how to implement it or make statements concerning the complexity of decoding. Our proof makes similar assumptions as the Kovalev-Pryadko QLDPC threshold theorem [38] where they assumed a minimum weight decoder without addressing implementation issues. Indeed, decoding for arbitrary LDPC codes is an NP-complete problem that we do not expect to be efficiently solvable in full generality.

Definition 3 (Ball decoder). *The Ball decoder has variable parameter $t > 0$. Given an observed syndrome $S = \sigma(E) + S_e$ where S_e is the syndrome error, the Ball decoder of parameter t performs the following 2 steps*

1. *Syndrome repair: find S_r of minimum weight $|S_r|$ such that $S + S_r$ belongs to Ball_t , where*

$$\text{Ball}_t = \{\sigma(E) \mid |E| \leq t\}.$$

2. *Qubit decode: find E_r of minimum weight $|E_r|$ such that $\sigma(E_r) = S + S_r$.*

We call $R = E + E_r$ the residual error.

A key result in proving Theorem 1 is the following promise on the performance of the Ball decoder: when a code has confinement, the weight of the residual error after one decoding cycle is bounded by a function of the weight of the syndrome error.

Lemma 1. *Consider a stabiliser code that has (t, f) -confinement. Provided that the original error pattern E has $|E|_{\text{red}} \leq t/2$, on input the observed syndrome $S = \sigma(E) + S_e$, the residual error R left by the Ball decoder of parameter $t/2$ satisfies:*

$$|R|_{\text{red}} \leq f(2|S_e|). \quad (7)$$

Proof. Assume $|E|_{\text{red}} \leq t/2$. By construction, E_r has minimum weight among all errors in $\text{Ball}_{t/2}$. In particular $|E_r| \leq t/2$. By the triangular inequality for the weight function,

$$|E + E_r|_{\text{red}} \leq |E|_{\text{red}} + |E_r|_{\text{red}} \leq t. \quad (8)$$

Therefore, we can apply the confinement property on the residual error $R = E + E_r$:

$$f(|\sigma(E + E_r)|) \geq |E + E_r|_{\text{red}}. \quad (9)$$

By linearity of the syndrome function $\sigma(\cdot)$:

$$\sigma(E + E_r) = \sigma(E) + \sigma(E_r) = S_e + S_r. \quad (10)$$

Note that the syndrome error S_e is a possible solution of the syndrome repair step of the Ball decoder, because by assumption $|E|_{\text{red}} \leq t/2$. Thus, $|S_r| \leq |S_e|$ and so

$$|S_e + S_r| \leq |S_e| + |S_r| \leq 2|S_e| \quad (11)$$

Combining these and the monotonicity of f leads to the required bound on the residual error:

$$|E + E_r|_{\text{red}} \leq f(2|S_e|). \quad (12)$$

□

Theorem 1 follows directly from Lemma 1. In particular, Lemma 1 entails that a code with (t, f) -confinement is robust against N cycles of qubit noise, noisy syndrome extraction and single-shot decoding as explained below.

At each cycle τ , we assume that a new error E^τ is introduced in the system and it is added to the residual error $R^{\tau-1}$. We assume that for the new physical error E^τ and the syndrome measurement error S_e^τ the following hold:

$$|E^\tau|_{\text{red}} \leq t/4 \quad \text{and} \quad f(2|S_e^\tau|) \leq t/4. \quad (13)$$

We perform syndrome extraction on the state $\hat{E}^\tau = R^{\tau-1} + E^\tau$. The noisy syndrome $S^\tau = \sigma(\hat{E}^\tau) + S_e^\tau$ is used as input for the Ball decoder of parameter $t/2$. The recovery operator E_r^τ found by the Ball decoder is then applied to the state and finally a new cycle starts where $R^\tau = \hat{E}^\tau + E_r^\tau$. Let $R^0 = 0$, so that the initial state of the system is given by $\hat{E}^1 = E^1$, $S^1 = \sigma(\hat{E}^1) + S_e^1$. Note that if

$$|E^\tau|_{\text{red}}, |R^{\tau-1}|_{\text{red}} \leq t/4 \quad (14)$$

then $|\hat{E}^\tau|_{\text{red}} = |E^\tau + R^{\tau-1}|_{\text{red}} \leq t/2$ and the hypotheses of Lemma 1 hold. Combining this with the bound on the syndrome error (13), we obtain

$$|R^\tau| \leq f(2|S_e^\tau|) \leq \frac{t}{4}.$$

In conclusion, provided that the conditions on the physical and the measurement error (13) are satisfied for each iteration up to $\tau - 1$, the residual error after the τ^{th} cycle is kept under control too.

The proof of Theorem 2 is very technical and is deferred to App. B. It is an adaption of the one of soundness for 4D codes given in [18], and it is reported in this manuscript for completeness.

We remind the reader that, for our numerical studies, we do not use the Ball decoder, but rather heuristics that perform well in practice. In particular, we use a two-stage decoder that exploits a metacheck structure on syndromes and attempts to repair the syndrome if and only if it does not pass all metachecks.

Our main motivation to introduce the concept of confinement and the Ball decoder was, in fact, to find a feature of codes able to encompass all known examples of single-shot codes. Campbell [18] introduced the notion of soundness and showed that this property is a sufficient condition for codes to show single-shot properties in the adversarial setting. Nonetheless, Fawzi et al. [22] showed that expander codes have a single-shot threshold for local stochastic noise, even though they do not have the soundness property. As already said though, expander codes do have confinement. In Corollary 9 of [20] the authors prove that their confinement function is linear and call this property *robustness*. Confinement, in other words, fills the gap leaved by the concept of soundness. Furthermore, as Lemma 2 states, it is a requirement strictly weaker than soundness: any LDPC family of codes with good soundness has good confinement.

Definition 4 (Soundness [18]). *Let t be an integer and $f : \mathbb{Z} \rightarrow \mathbb{R}$ be a function with $f(0) = 0$. Given a stabiliser code with syndrome map $\sigma(\cdot)$ we say it is (t, f) -sound if for all error sets E with $|\sigma(E)| \leq t$ it follows that $f(|\sigma(E)|) \geq |E|_{\text{red}}$.*

Definition 5 (Good soundness [18]). *Consider an infinite family of codes with syndrome maps $\sigma_n(\cdot)$. We say that the family has good soundness if each code in it is (t, f) -sound where:*

1. t grows with n such that $t \in \Omega(n^b)$ with $b > 0$;

2. and $f(\cdot)$ is monotonically increasing and independent of n .

It follows easily from Campbell's definition of soundness and our definition of confinement that the former entails the latter.

Lemma 2. *Consider a LDPC code that is (t, f) -sound with f increasing. If its qubit degree is at most ω , then it has $(\frac{t}{\omega}, f)$ -confinement.*

Proof. If E is an error set with $|E|_{\text{red}} \leq \frac{t}{\omega}$, for its syndrome the following holds:

$$|\sigma(E)| \leq \frac{t}{\omega} \cdot \omega = t. \quad (15)$$

By soundness of the code:

$$f(|\sigma(E)|) \geq |E|_{\text{red}}. \quad (16)$$

□

In conclusion, confinement does answer to the need of finding general and inclusive properties related to single-shot error correction.

V. NUMERICS

To assess the single-shot performance of the 3D product codes, we simulate the decoding of phase-flip (Z) errors. As 3D product codes are CSS codes, the relevant stabilizers are the X stabilizers. Let $e_Z \in \mathbb{F}_2^n$ describe the support of a phase-flip error, i.e. $(e_Z)_i = 1$ if qubit i has a phase-flip error. The syndrome, s_X , of this error is then

$$s_X = H_X e_Z, \quad (17)$$

where $H_X \in \mathbb{F}_2^{m \times n}$ is the parity check matrix of the X stabilizers of the code (see Eq. (3)).

Owing to the chain-complex structure of 3D product codes (outlined in Sec. III) the syndromes s_X are themselves the codewords of a classical linear code with parity check matrix M such that $M s_X = 0$ for all $s_X \in \text{Im}(H_X)$. We refer to such a code on the syndromes as metacode. The metacheck matrix can be used to detect and correct syndrome noise.

In a two-stage single-shot decoder, stage 1 decoding corrects the syndrome noise using M before stage 2 decoding corrects the data qubits. In general, decoding is an NP-complete problem that cannot be solved exactly in polynomial-time. However, good heuristic techniques exist that allow approximate solutions to be efficiently computed. In this work, we use two such decoding methods: minimum weight perfect matching (MWPM) and belief propagation plus ordered statistics decoding (BP+OSD). Both MWPM and BP+OSD are algorithms that run over graphical models that encapsulate the structure of the code. We now briefly describe each decoder.

A. Minimum weight perfect matching (MWPM)

The minimum weight perfect matching (MWPM) decoder is useful for codes that produce pairs of syndromes at the ends of error chains. The method works by mapping the decoding problem to a graphical model in which nodes represent the code syndromes and weighted edges represent error chains of different lengths. For a given pair of syndrome excitations, the MWPM algorithm deduces the shortest error chain that could have caused it [39].

MWPM finds use for a variety of topological codes, most famously for the 2D surface and toric codes [2, 40–43]. For 3D codes, MWPM is a suitable candidate for syndrome repair step referred to as stage 1 decoding. Specifically, the syndrome of a phase-flip error can be viewed as a collection of closed loops of edges in a simple cubic lattice¹ (with boundary conditions depending on the code). Measurement errors cause loops of syndrome to be broken, and the job of stage 1 decoding is to repair these broken syndromes. To obtain the corresponding matching problem, we create a complete graph whose vertices correspond to the break-points of the broken syndrome loops, with edge weights that are equal to the path lengths between the break-points. We use the Blossom V [44] implementation of Edmonds’s algorithm to solve this matching problem. The edges in the matching correspond to the syndrome recovery operators.

B. Belief propagation + ordered statistics decoding (BP+OSD)

Belief propagation (BP) is an algorithm for performing inference on sparse graphs that finds widespread use in high-performance classical coding. Classical LDPC codes, for example, achieve performance close to the Shannon-limit when decoded with BP [45]. In the context of quantum coding, BP is useful for codes that do not produce pairs of syndromes and therefore cannot be decoded with MWPM.

The BP algorithm maps the decoding problem to a bipartite *factor graph* where the two node species represent data qubits and syndromes respectively. Graph edges are drawn between the data and syndrome nodes according to the code’s parity check matrix. The factor graph is designed to provide a factorisation of the probability distribution that describes the relationship between syndromes and errors. The BP algorithm proceeds by iteratively passing ‘beliefs’ between data and syndrome nodes, at each step updating the probability that a data node is errored. The algorithm terminates once the probability distribution implies a error pattern that satisfies the inputted syndrome.

For quantum codes, the standard BP algorithm alone does not achieve good decoding performance due to the presence of degenerate errors. These cause ‘split-beliefs’ and prevent the algorithm from terminating. Fortunately, the problem of split-beliefs can be resolved by incorporating a post-processing

technique known as ordered statistics decoding (OSD). The OSD step uses the probability distribution outputted by BP to select a low-weight recovery operator that satisfies the syndrome equation.

The BP+OSD algorithm was first applied to quantum expander codes by Panteleev and Kalachev [46]. Following this, Roffe et al. [47] demonstrated that the BP+OSD decoder applies more widely across a broad range of QLDPC codes, including the 2D surface and toric codes. For this work, we use the software implementation of BP+OSD from [47], which can be downloaded from [48].

C. The two-stage single-shot decoding algorithm

Our simulations of the two-stage single shot decoder employ two strategies. 1) MWPM & BP+OSD: stage 1 decoding is performed using MWPM and stage 2 decoding uses BP+OSD. 2) BP+OSD \times 2: both stages are BP+OSD.

Algorithm 1 describes our methodology for the simulations of the two-stage single-shot decoder.

Algorithm 1 SINGLE-SHOT ERROR CORRECTION

Input: Decoder 1, decoder 2, number of rounds N , error rate p , X parity check matrix H_X , metacheck matrix M , modified metacheck matrix M'

Output: Success or failure

```

1:  $e_Z \leftarrow 0$  ▷ Qubit error
2:  $s_X \leftarrow 0$  ▷ Syndrome
3:  $m \leftarrow 0$  ▷ Metasyndrome
4: for  $j \leftarrow 1$  to  $N$  do
5:   Generate phase-flip error  $e'_Z$  according to error rate  $p$ 
6:    $e_Z \leftarrow e_Z + e'_Z$ 
7:    $s_X \leftarrow H_X e_Z$ 
8:   Generate syndrome error  $s'_X$  according to error rate  $p$ 
9:    $s_X \leftarrow s_X + s'_X$ 
10:   $m \leftarrow M s_X$ 
11:  Use decoder 1 to obtain syndrome recovery  $r_M$  such that
       $M r_M = m$ 
12:   $s_X \leftarrow s_X + r_M$ 
13:  if  $s_X \notin \text{Im}(H_X)$  then ▷ Failure-mode subroutine
14:     $s_X \leftarrow s_X + r_M$ 
15:    Use decoder 1 to obtain valid  $r_M$  s.t.  $M' r_M = m$ 
16:     $s_X \leftarrow s_X + r_M$ 
17:  end if
18:  Use decoder 2 to obtain qubit recovery  $r_Z$  s.t.  $H_X r_Z = s_X$ 
19:   $e_Z \leftarrow e_Z + r_Z$ 
20: end for
21: Generate phase-flip error  $e'_Z$  according to error rate  $p$ 
22:  $e_Z \leftarrow e_Z + e'_Z$ 
23:  $s_X \leftarrow H_X e_Z$ 
24: Use decoder 2 to obtain qubit recovery  $r_Z$  s.t.  $H_X r_Z = s_X$ 
25:  $e_Z \leftarrow e_Z + r_Z$ 
26: if  $e_Z$  is a stabiliser then
27:   return Success
28: end if
29: return Failure

```

The 3D toric code has a failure mode that is not present in the 3D surface code. In such codes, syndromes s_X exist

¹ Namely, the dual lattice of the one described in App. A.

that satisfy all of the metachecks, $M s_X = 0$, but are *invalid* syndromes, meaning that s_X does not belong to the image of H_X . In other words, s_X is invalid if there is no error vector $e_Z \in \mathcal{C}_1$ with syndrome s_X but it is a codeword of the metacode. Referring to the chain complex structure of \mathcal{C} :

$$\mathcal{C}_0 \xrightarrow{H_Z^T} \mathcal{C}_1 \xrightarrow{H_X} \mathcal{C}_2 \xrightarrow{M} \mathcal{C}_3$$

we see that these non-valid syndromes are non-trivial elements of the 2nd homology group:

$$\mathcal{H}_2 = \ker \delta_2 / \text{Im } \delta_1 = \ker M / \text{Im } H_X.$$

If k_m is the dimension of \mathcal{H}_2 , the set of invalid syndromes is a vector subspace of \mathcal{C}_2 of dimension k_m whose vectors can be written as $u + H_X e_Z$ where u is a representative of the equivalence class $[u] \in \mathcal{H}_2$ and $e_Z \in \mathcal{C}_1$. Thus, if F_M is a matrix whose columns are k_m vectors in \mathcal{C}_2 that generate \mathcal{H}_2 (meaning that they belong to k_m different equivalence classes in \mathcal{H}_2), we can write any invalid syndrome s_X as:

$$s_X = F_M v + H_X e_Z, \quad (18)$$

where $v \in \mathbb{F}_2^{k_m}$ is non-zero if and only if s_X is invalid and e_Z is any error vector in \mathcal{C}_1 .

By duality on \mathcal{C} , the 2nd cohomology group:

$$\mathcal{H}_2^* = \ker \delta_1^T / \text{Im } \delta_2^T = \ker H_X^T / \text{Im } M^T,$$

has order k_m too. If L_M is a matrix whose k_m rows generates \mathcal{H}_2^* , then the product $\Pi = L_M F_M$ has full rank k_m because both L_M and F_M have full rank. Moreover, since the rows of L_M in particular belongs to $\ker H_X^T$, it holds $L_M H_X = 0$. Combining these two observations with Eq. (18) yields:

$$\begin{aligned} L_M s_X &= L_M F_M v + L_M H_X e_Z \\ &= \Pi v \end{aligned}$$

where $\Pi v = 0$ if and only if $v = 0$ because Π is full rank. In conclusion, we have found that:

$$L_M s_X \neq 0$$

if and only if s_X is an invalid syndrome. As a consequence, we can assess whether a syndrome is invalid or not by calculating this product. The meaning of matrices L_M and F_M can be understood by looking at elements in \mathcal{H}_2 and \mathcal{H}_2^* as logical operators of a CSS code defined on \mathcal{C} with qubits in \mathcal{C}_2 (see Sec. III). In this settings, the full rank condition $\text{rank}(L_M F_M) = k_m$ translates in the anticommuting relation between logical X and logical Z operators of the code.

In the 3D toric code, these invalid syndromes are loops of edges around one of the handles of the torus, and are equivalent to the logical operators of the metacode. It is therefore possible to check whether stage 1 decoding results in such a failure by checking whether the repaired syndrome anticommutes with a basis L_M of the relevant logical operators of the metacode. When a metacode failure is encountered, a failure-mode subroutine (line 13 of Algorithm 1) is called that

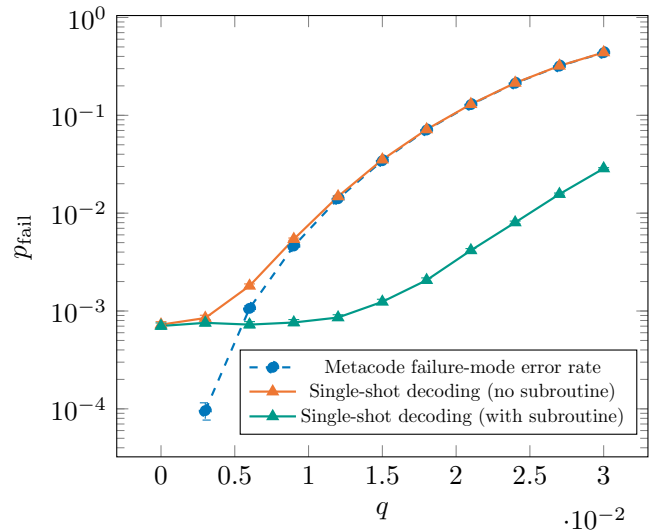


FIG. 2. Single-shot decoding of the 3D toric code with $L = 5$, with and without the metacode failure-mode subroutine. The failure rate p_{fail} is plotted against increasing values of the syndrome error rate q , whilst the phase-flip error rate is set to $p = 0.1$. Without the subroutine, the single-shot decoder rapidly converges to the failure-mode error rate (dotted line). For large values of q the subroutine improves the logical failure rate by over an order of magnitude. In this simulation, BP+OSD was used for both stage 1 and 2 decoding.

forces the repaired syndrome into the correct form. This subroutine involves using BP+OSD to decode a modified version of the metacheck matrix M' defined as follows

$$M' = \begin{pmatrix} M \\ L_M \end{pmatrix}. \quad (19)$$

The additional constraints in the modified metacheck matrix ensures that the repaired syndrome is never an invalid syndrome. We call this procedure as a subroutine (rather than all the time) as the L_M component causes M' to have higher maximum row and column weights than M , resulting in a reduction in BP decoding performance. Indeed, the rows of L_M must have weight lower bounded by the transpose distances of the seed codes². Since the transpose distances of the seed codes also determine the Z -distance of the quantum code (Sec. III), we want these quantities to be growing with the length n of the code and therefore the matrix L_M is not, in general, LDPC.

We find that whilst the failure-mode subroutine does not change the error threshold of the decoder, it does considerably reduce the logical error rate. This is illustrated by Fig. 2, which shows the single-shot logical error rate with and without the failure-mode subroutine. For large syndrome error rates, Fig. 2 shows the failure-mode subroutine improves decoding performance by over an order of magnitude.

² More precisely, rows of L_M are vectors in \mathcal{C}_2 that correspond to elements of the second cohomology group \mathcal{H}_2^* ; hence their weight is lower bounded by $d_2^* = \min\{d_a^T d_b^T, d_a^T d_c^T, d_b^T d_c^T\}$, see [37].

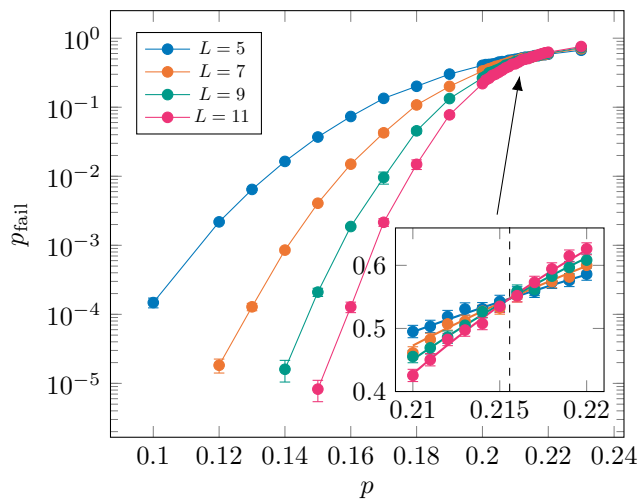


FIG. 3. Code capacity threshold of the 3D toric code. We plot the logical error rate p_{fail} as a function of the phase-flip error rate p for codes with linear lattice size L . The inset shows a zoom of the threshold region, where the lines show the threshold fit described in Appendix C. All data points have at least 25 failure events. The error bars show the 95% confidence intervals $p_{\text{fail}} = \hat{p}_{\text{fail}} \pm 1.96\sqrt{p_{\text{fail}}(1-p_{\text{fail}})/\eta}$, where $\eta \geq 10^4$ is the number of Monte Carlo trials.

D. 3D toric and surface codes

We estimate the sustainable threshold of the 3D toric and surface codes using our two decoding strategies. For code-capacity noise (i.e. perfect syndrome measurements), the syndrome-repair step is not required, so both decoding strategies are the same. For each code family, we observe a code capacity threshold of $p_{\text{th}} \approx 21.6\%$, as illustrated in Fig. 3. To obtain our threshold estimates, we use the standard critical exponent method [49] (see Appendix C for details). In the single-shot setting, we find similar performance for both our decoding strategies, as summarized in Table II. Our results compare favourably with the performance of other decoders, which we list in Table I. We obtain the highest reported code-capacity threshold and the highest reported single-shot threshold.

We remark that the sustainable threshold that we observe for the 3D toric code is very close to the threshold of MWPM for string-like errors in the 3D toric code [50]. This implies that the performance of decoder 1 (the syndrome-repair step) is limiting the performance of the entire decoding procedure, as was suggested in [13]. Although the sustainable thresholds we observe for 3D surface codes are slightly higher than for 3D toric codes, the codes we consider are relatively small, which means that boundary effects may be having an impact on our sustainable threshold estimates.

We also investigated the suppression of the logical error rate below threshold in the 3D toric code, using MWPM & BP+OSD. We use the following ansatz for the logical error rate for values of $p < p_{\text{th}}$,

$$p_{\text{fail}}(L) \propto (p/p_{\text{th}})^{\alpha L^\beta}, \quad (20)$$

where α and β are parameters to be determined. The code distance of the 3D toric code for Z errors is L^2 , so if the decoder is correcting errors up to this size, we would expect $\beta \approx 2$. Using the fitting procedure described in Appendix C, we estimate $\beta = 1.91(3)$ for $N = 0$ (code capacity) and $\beta = 1.15(3)$ for $N = 8$ (eight rounds of single-shot error correction). Therefore, for the (relatively small) codes that we consider, we find evidence that BP+OSD is correcting errors of weight up to the code distance. Viewed as an error correction problem, the distance of the syndrome-repair step of decoding (i.e the single-shot distance d_{ss}) is L , which is consistent of our observed value of β in the single-shot case. This provides further evidence that the bottle-neck of our single-shot decoding procedure is the syndrome-repair step.

E. Non-topological codes

So far, we have focused on the decoding of 3D topological codes. We now show that the BP+OSD decoder can be used for single-shot decoding of more general 3D product codes. Table III shows a family 3D product codes constructed by taking the 3D product of a $(3, 4)$ -LDPC code with two instances of the classical repetition code. The result is a code family where the number of logical qubits is not fixed. This code family was decoded using a two-stage single-shot decoder, BP+OSD $\times 2$, yielding the threshold plot in Fig. 4. The simulation results suggest a sustainable threshold in the region of 2.7%.

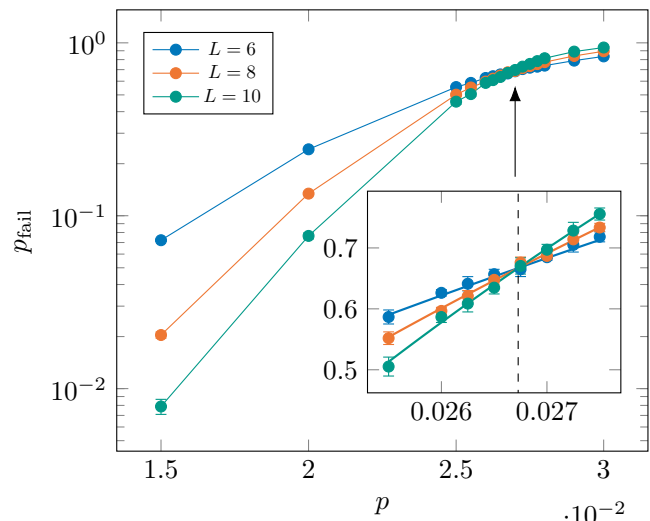


FIG. 4. Threshold plot for a family of non-topological 3D product codes after 16 rounds of single-shot error correction using the BP+OSD decoder. The simulation results suggest a threshold at 2.7%. The error bars show the 95% confidence intervals $p_{\text{fail}} = \hat{p}_{\text{fail}} \pm 1.96\sqrt{p_{\text{fail}}(1-p_{\text{fail}})/\eta}$, where η is the number of Monte Carlo trials.

VI. CONCLUSION

In this article, we investigated single-shot decoding of 3D product codes. We gave a formal definition of confinement in quantum codes and proved that all 3D product codes have confinement for Z errors. We also proved that confinement is sufficient for single-shot error correction against adversarial noise. This is a strengthening of the result of Campbell [18], who showed that a property called soundness is sufficient for single-shot error correction, in that soundness implies confinement but the converse is not true. Remarkably, there are important classes of codes, such as quantum expander codes, which have confinement but not soundness. The obvious open problem arising from our work is how to extend our findings to the local stochastic noise model. Is confinement a sufficient condition for LDPC codes to exhibit a single-shot threshold? If not, what other requirements should a code satisfy to ensure the existence of a single-shot threshold?

We simulated single-shot error correction for a variety of 3D product codes, concentrating on 3D toric and surface codes. Using MWPM & BP+OSD, we achieved the best known code capacity error threshold and sustainable single-shot error threshold for this code family (for phase-flip noise). Our results strongly suggest that the bottleneck of two-stage decoders is the first stage where the noisy syndrome is repaired. For the 3D toric code, the optimal threshold of the syn-

drome repair step is 3.3% [33], whereas the optimal threshold of the entire decoding problem is 11.0% [35]. This implies that two-stage decoders can never achieve optimal performance in these codes, so perhaps other single-shot decoding methods ought to be investigated in future.

We also simulated single-shot error correction for a family of non-topological 3D product codes, using BP+OSD for both decoding steps. We achieved performance very close to that of the 3D toric and surface codes, which indicates that BP+OSD is a high-performance single-shot decoder. Furthermore, the versatility of BP+OSD means that we expect it to work as a single-shot decoder for general LDPC 3D product codes. We leave confirmation of this to future work, and we conjecture that BP+OSD will achieve good performance for other classes of QLDPC codes such as topological fracton codes [51, 52].

Acknowledgements.- This work was supported by the Engineering and Physical Sciences Research Council [grant numbers EP/P510270/1 (J.R.S.) and EP/M024261/1 (E.T.C. and J.R.)]. M.V. thanks Aleksander Kubica and Nikolas Breuckmann for illuminating discussions. Research at Perimeter Institute is supported in part by the Government of Canada through the Department of Innovation, Science and Economic Development Canada and by the Province of Ontario through the Ministry of Colleges and Universities. This research was enabled in part by support provided by Compute Ontario (www.computeontario.ca) and Compute Canada (www.computecanada.ca). This work was completed while ETC was at the University of Sheffield.

-
- [1] Joschka Roffe. Quantum error correction: an introductory guide. *Contemporary Physics*, 60(3):226–245, 2019.
 - [2] Eric Dennis, Alexei Kitaev, Andrew Landahl, and John Preskill. Topological quantum memory. *Journal of Mathematical Physics*, 43(9):4452–4505, 2002.
 - [3] Austin G. Fowler, Ashley M. Stephens, and Peter Groszkowski. High-threshold universal quantum computation on the surface code. *Phys. Rev. A*, 80:052312, 2009.
 - [4] R Raussendorf, J Harrington, and K Goyal. Topological fault-tolerance in cluster state quantum computation. *New Journal of Physics*, 9(6), 2007.
 - [5] A Bolt, G Duclos-Cianci, D Poulin, and TM Stace. Foliated quantum error-correcting codes. *Physical review letters*, 117(7):070501, 2016.
 - [6] Naomi Nickerson and Héctor Bombín. Measurement based fault tolerance beyond foliation. *arXiv preprint arXiv:1810.09621*, 2018.
 - [7] Hector Bombin. 2D quantum computation with 3D topological codes. *arXiv preprint arXiv:1810.09571*, 2018.
 - [8] Benjamin J Brown. A fault-tolerant non-Clifford gate for the surface code in two dimensions. *arXiv preprint arXiv:1903.11634*, 2019.
 - [9] Michael Newman, Leonardo Andreta de Castro, and Kenneth R Brown. Generating fault-tolerant cluster states from crystal structures. *arXiv preprint arXiv:1909.11817*, 2019.
 - [10] Héctor Bombín. Single-shot fault-tolerant quantum error correction. *Phys. Rev. X*, 5(3):031043, 2015.
 - [11] Héctor Bombín. Resilience to time-correlated noise in quantum computation. *Phys. Rev. X*, 6(4):041034, 2016.
 - [12] Benjamin J. Brown, Naomi H. Nickerson, and Dan E. Browne. Fault-tolerant error correction with the gauge color code. *Nat Commun*, 7, 2016.
 - [13] Kasper Duivenvoorden, Nikolas P Breuckmann, and Barbara M Terhal. Renormalization group decoder for a four-dimensional toric code. *IEEE Transactions on Information Theory*, 65(4):2545–2562, 2018.
 - [14] Nikolas P Breuckmann and Vivien Londe. Single-shot decoding of linear rate LDPC quantum codes with high performance. *arXiv preprint arXiv:2001.03568*, 2020.
 - [15] Aleksander Kubica. *The ABCs of the Color Code: A Study of Topological Quantum Codes as Toy Models for Fault-Tolerant Quantum Computation and Quantum Phases Of Matter*. PhD thesis, Caltech, 2018.
 - [16] Aleksander Kubica and John Preskill. Cellular-Automaton Decoders with Provable Thresholds for Topological Codes. *Physical Review Letters*, 123(2):020501, 2019.
 - [17] Michael Vasmer, Dan E Browne, and Aleksander Kubica. Cellular automaton decoders for topological quantum codes with noisy measurements and beyond. *arXiv preprint arXiv:2004.07247*, 2020.
 - [18] Earl T Campbell. A theory of single-shot error correction for adversarial noise. *Quantum Science and Technology*, 4(2):025006, 2019.
 - [19] Jean-Pierre Tillich and Gilles Zémor. Quantum LDPC codes with positive rate and minimum distance proportional to the square root of the blocklength. *IEEE Transactions on Information Theory*, 60(2):1193–1202, 2014.
 - [20] Anthony Leverrier, Jean-Pierre Tillich, and Gilles Zémor.

- Quantum expander codes. In *Foundations of Computer Science (FOCS), 2015 IEEE 56th Annual Symposium on*, pages 810–824. IEEE, 2015.
- [21] Omar Fawzi, Antoine Groppe, and Anthony Leverrier. Efficient decoding of random errors for quantum expander codes. In *Proc. STOC*, pages 521–534. ACM, 2018.
- [22] Omar Fawzi, Antoine Groppe, and Anthony Leverrier. Constant overhead quantum fault tolerance with quantum expander codes. to appear in FOCS 2018, 2018.
- [23] Austin G Fowler. Time-optimal quantum computation. *arXiv preprint arXiv:1210.4626*, 2012.
- [24] Barbara M Terhal. Quantum error correction for quantum memories. *Rev. Mod. Phys.*, 87(2):307, 2015.
- [25] Poulami Das, Christopher A. Pattison, Srilatha Manne, Douglas Carmean, Krysta Svore, Moinuddin Qureshi, and Nicolas Delfosse. A Scalable Decoder Micro-architecture for Fault-Tolerant Quantum Computing. *arXiv preprint arXiv:2001.06598*, pages 1–19, 2020.
- [26] Antoine Groppe and Anirudh Krishna. Numerical study of hypergraph product codes. *arXiv preprint arXiv:1810.03681*, 2018.
- [27] Antoine Groppe, Lucien Grouès, Anirudh Krishna, and Anthony Leverrier. Combining hard and soft decoders for hypergraph product codes. *arXiv preprint arXiv:2004.11199*, 2020.
- [28] Sergey Bravyi and Matthew B Hastings. Homological product codes. In *Proceedings of the 46th Annual ACM Symposium on Theory of Computing*, pages 273–282. ACM, 2014.
- [29] Benjamin Audoux and Alain Couvreur. On tensor products of CSS codes. *arXiv preprint arXiv:1512.07081*, 2015.
- [30] Arun B. Alosi and Pradeep Kiran Sarvepalli. Decoding toric codes on three dimensional simplicial complexes. *arXiv preprint arXiv:1911.06056*, 2019.
- [31] Nikolas P. Breuckmann and Xiaotong Ni. Scalable Neural Network Decoders for Higher Dimensional Quantum Codes. *Quantum*, 2:68, 2018.
- [32] Yukiyasu Ozeki and Nobuyasu Ito. Multicritical dynamics for the $\pm J$ Ising model. *Journal of Physics A: Mathematical and General*, 31(24):5451–5461, 1998.
- [33] Takuya Ohno, Gaku Arakawa, Ikuo Ichinose, and Tetsuo Matsui. Phase structure of the random-plaquette \mathbb{Z}_2 gauge model: Accuracy threshold for a toric quantum memory. *Nuclear Physics B*, 697:462–480, 2004.
- [34] Martin Hasenbusch, Francesco Parisen Toldin, Andrea Pelissetto, and Ettore Vicari. Magnetic-glassy multicritical behavior of the three-dimensional $\pm J$ Ising model. *Physical Review B - Condensed Matter and Materials Physics*, 76(18):184202, 2007.
- [35] Koujin Takeda and Hidetoshi Nishimori. Self-dual random-plaquette gauge model and the quantum toric code. *Nuclear Physics B*, 686(3):377–396, 2004.
- [36] Aleksander Kubica, Michael E. Beverland, Fernando Brandão, John Preskill, and Krysta M. Svore. Three-Dimensional Color Code Thresholds via Statistical-Mechanical Mapping. *Physical Review Letters*, 120(18):180501, 2018.
- [37] Weilei Zeng and Leonid P. Pryadko. Higher-dimensional quantum hypergraph-product codes with finite rates. *Phys. Rev. Lett.*, 122:230501, 2019.
- [38] Alexey A. Kovalev and Leonid P. Pryadko. Fault tolerance of quantum low-density parity check codes with sublinear distance scaling. *Phys. Rev. A*, 87:020304, 2013.
- [39] Jack Edmonds. Paths, trees, and flowers. *Canadian Journal of mathematics*, 17:449–467, 1965.
- [40] Austin G. Fowler, Matteo Mariantoni, John M. Martinis, and Andrew N. Cleland. Surface codes: Towards practical large-scale quantum computation. *Phys. Rev. A*, 86:032324, 2012.
- [41] Nikolas P Breuckmann and Barbara M Terhal. Constructions and noise threshold of hyperbolic surface codes. *IEEE Transactions on Information Theory*, 62(6):3731–3744, 2016.
- [42] Benjamin J. Brown and Dominic J. Williamson. Parallelized quantum error correction with fracton topological codes. *Phys. Rev. Research*, 2:013303, 2020.
- [43] Aleksander Kubica and Nicolas Delfosse. Efficient color code decoders in $d \geq 2$ dimensions from toric code decoders. *arXiv preprint arXiv:1905.07393*, 2019.
- [44] Vladimir Kolmogorov. Blossom V: A new implementation of a minimum cost perfect matching algorithm. *Mathematical Programming Computation*, 1(1):43–67, 2009.
- [45] David JC MacKay and Radford M Neal. Near shannon limit performance of low density parity check codes. *Electronics letters*, 33(6):457–458, 1997.
- [46] Pavel Panteleev and Gleb Kalachev. Degenerate quantum LDPC codes with good finite length performance. *arXiv preprint arXiv:1904.02703*, 2019.
- [47] Joschka Roffe, David R White, Simon Burton, and Earl T Campbell. Decoding across the quantum LDPC code landscape. *arXiv preprint arXiv:2005.07016*, 2020.
- [48] Joschka Roffe. BP+OSD - a decoder for sparse quantum codes. *github.com*.
- [49] J Harrington. *Analysis of quantum error-correcting codes: symplectic lattice codes and toric codes*. PhD thesis, Caltech, 2004.
- [50] Chenyang Wang, Jim Harrington, and John Preskill. Confinement-higgs transition in a disordered gauge theory and the accuracy threshold for quantum memory. *Annals of Physics*, 303(1):31–58, 2003.
- [51] Sagar Vijay, Jeongwan Haah, and Liang Fu. Fracton topological order, generalized lattice gauge theory, and duality. *Phys. Rev. B*, 94:235157, 2016.
- [52] Arpit Dua, Isaac H. Kim, Meng Cheng, and Dominic J. Williamson. Sorting topological stabilizer models in three dimensions. *Phys. Rev. B*, 100:155137, 2019.

Appendix A: Qubit placement on a 3D lattice

Here we detail how to embed a 3D product code on a cubic lattice, where qubits sit on edges, Z -stabilisers on vertices, X -stabilisers on faces and metachecks on cells.

Let C^0 and C^1 be two vector spaces over \mathbb{F} with basis $\mathcal{B}^0 = \{e_1^0, \dots, e_n^0\}$ and $\mathcal{B}^1 = \{e_1^1, \dots, e_m^1\}$ respectively. Given a linear map from C^0 into C^1 , it can be represented as a $m \times n$ matrix δ over \mathbb{F} such that its action on the elements of the basis \mathcal{B}^0 is given by:

$$\delta : C^0 \longrightarrow C^1$$

$$e_i^0 \longmapsto \delta e_i^0 = \sum_{\alpha=1}^m \delta_{\alpha,i} e_{\alpha}^1. \quad (\text{A1})$$

Expression (A1) allows us to write the support of vectors in $\delta(\mathcal{B}^0) = \{\delta e_i^0\}_i$ in a compact form. In fact, the support of δe_i^0 is the subset of \mathcal{B}^1 :

$$\text{supp}(\delta e_i^0) = \{e_{\alpha}^1 \mid \delta_{\alpha,i} \neq 0\}_{\alpha}.$$

Since basis vectors are uniquely identified by their index, we can compactly write (A1) as a relation $*$ on the set of indices

of the basis \mathcal{B}^0 and \mathcal{B}^1 :

$$\begin{aligned} \{1, \dots, n\} &\longrightarrow \{1, \dots, m\} \\ \kappa &\longrightarrow \kappa^*, \end{aligned} \quad (\text{A2})$$

where

$$\kappa^* = \{\eta \mid \delta_{\eta, \kappa} \neq 0\}_\eta.$$

Similarly, the transpose δ^T of the matrix δ induces a map from C^1 to C^0 which is defined on \mathcal{B}^1 as

$$\begin{aligned} \delta^T : C^1 &\longrightarrow C^0 \\ e_\alpha^1 &\longmapsto \delta^T e_\alpha^1 = \sum_{i=1}^n \delta_{\alpha, i} e_i^0, \end{aligned}$$

yields the relation on indices

$$\begin{aligned} \{1, \dots, m\} &\longrightarrow \{1, \dots, n\} \\ \eta &\longrightarrow \eta^*, \end{aligned} \quad (\text{A2 T})$$

where

$$\eta^* = \{\kappa \mid \delta_{\eta, \kappa} \neq 0\}_\kappa.$$

Referring to the chain complex \mathcal{C} described in Sec. III, we choose bases $\mathcal{B}_\ell^r = \{e_{i^\tau}^r\}_i$ of C_ℓ^r for $\tau = 0, 1$ and $\ell = A, B, C$. We accordingly fix matrix representations of the maps δ_A, δ_B and δ_C ; with slight abuse of notation, we indicate with the same symbol the $m_\ell \times n_\ell$ matrix representation of a map and the map itself. We indicate with i, j, k indices of $\mathcal{B}_A^0, \mathcal{B}_B^0$ and \mathcal{B}_C^0 respectively and with α, β, γ indices of $\mathcal{B}_A^1, \mathcal{B}_B^1, \mathcal{B}_C^1$. Since we deal with 3-fold tensor product spaces (e.g. $C_A^0 \otimes C_B^0 \otimes C_C^0$) we consider triplets (i, j, k) of valid indices; we indicate with (i^*, j, k) the set of indices $\{(\eta, j, k) \mid \eta \in i^*\}$, and similarly for any possible triplet combination of starred (i^*) and non starred (i) indices.

As illustrated in Sec. III, when defining a CSS code on the chain complex \mathcal{C} , the following relations hold:

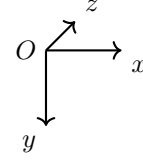
1. basis elements of \mathcal{C}_0 are in one-to-one correspondence with a generating set of Z -stabilisers;
2. basis elements of the vector space \mathcal{C}_1 are in one-to-one correspondence with the qubits;
3. basis elements of the vector space \mathcal{C}_2 are in one-to-one correspondence with a generating set of X -stabilisers;
4. basis elements of \mathcal{C}_3 are in one-to-one correspondence with a generating set of metachecks.

Combining these with (A2) and (A2 T), we obtain the relations reported in Table IV. More precisely, we choose as bases for the spaces $\mathcal{C}_3, \mathcal{C}_2, \mathcal{C}_1$ and \mathcal{C}_0 the product bases obtained by combining $\mathcal{B}_{\ell=A,B,C}^0$ and $\mathcal{B}_{\ell=A,B,C}^1$ and we index qubits, stabilisers and metachecks on \mathcal{C} accordingly. Equivalently, basis vectors are labelled with consecutive integers so as to preserve the ordering induced by the bases.

We use the relations of Table IV to visualise the chain complex \mathcal{C} on a 3D cubic lattice. In order to do so, we first fix a coordinate system

OBJECT	INDEXING	BASIS VECTOR
qubits	(α, j, k)	$(e_\alpha^{A_1} \otimes e_j^{B_0} \otimes e_k^{C_0}, 0, 0)$
	(i, β, k)	$(0, e_i^{A_0} \otimes e_\beta^{B_1} \otimes e_k^{C_0}, 0)$
	(i, j, γ)	$(0, 0, e_i^{A_0} \otimes e_j^{B_0} \otimes e_\gamma^{C_1})$
X -stabilisers	(α, β, k)	$\delta_2^T (e_\alpha^{A_1} \otimes e_\beta^{B_1} \otimes e_k^{C_0}, 0, 0)$
	(α, j, γ)	$\delta_2^T (0, e_\alpha^{A_1} \otimes e_j^{B_0} \otimes e_\gamma^{C_1}, 0)$
	(i, β, γ)	$\delta_2^T (0, 0, e_i^{A_0} \otimes e_\beta^{B_1} \otimes e_\gamma^{C_1})$
Z -stabilisers	(i, j, k)	$\delta_1 (e_i^{A_0} \otimes e_j^{B_0} \otimes e_k^{C_0})$
metacheck	(α, β, γ)	$\delta_3^T (e_\alpha^{A_1} \otimes e_\beta^{B_1} \otimes e_\gamma^{C_1})$

TABLE IV. Notation and correspondences between objects of the chain complex \mathcal{C} .



where O is the origin. Since basis vectors are labelled with integers (the i th basis vector corresponds to the integer i , and vice versa) we can build a 3D grid of points where any point corresponds to a basis vector of $\mathcal{C}_0, \mathcal{C}_1, \mathcal{C}_2$ or \mathcal{C}_3 . More precisely we fix a set of valid coordinates for points in the grid:

1. integer coordinates $(z, y, x) = (i, j, k)$ for $i = 1, \dots, n_a, j = 1, \dots, n_b$, and $k = 1, \dots, n_c$;
2. half-integers coordinates $(z, y, x) = (\alpha + 0.5, \beta + 0.5, \gamma + 0.5)$ for $\alpha = 1, \dots, m_a, \beta = 1, \dots, m_b$ and $\gamma = 1, \dots, m_c$;
3. the origin has coordinates $O = (1, 1, 1)$.

In this way, any point with valid coordinates uniquely identifies a basis vector (and therefore an object in the chain complex, see Table IV). For example:

1. the point $(1, 4, 2)$ corresponds to the basis vector $(e_1^{A_0} \otimes e_4^{B_0} \otimes e_2^{C_0}) \in \mathcal{C}_0$ (Z -stabilisers);
2. the point $(1.5, 4, 2)$ corresponds to the basis vector $(e_1^{A_1} \otimes e_4^{B_0} \otimes e_2^{C_0}, 0, 0) \in \mathcal{C}_1$ (qubits);
3. the point $(1.5, 4, 2.5)$ corresponds to the basis vector $(0, e_1^{A_1} \otimes e_4^{B_0} \otimes e_2^{C_1}, 0) \in \mathcal{C}_2$ (X -stabilisers);
4. the point $(1.5, 4.5, 2.5)$ corresponds to the basis vector $(e_1^{A_1} \otimes e_4^{B_1} \otimes e_2^{C_1}) \in \mathcal{C}_3$ (metachecks);

We draw an edge for any qubit of the code defined on \mathcal{C} . Qubits are in one-to-one correspondence with basis element of \mathcal{C}_1 and therefore are of three different types: $(v, 0, 0)$, $(0, v, 0)$ and $(0, 0, v)$. Accordingly, we draw edges of three different types as detailed in Table V (see also Fig. 5, 6). In other words, any point with two integer entries and one half integer entry is the middle point of an edge of unit length, which corresponds to a qubit. In this way we obtain a cubic lattice with (possibly) some missing edges.

QUBIT	EDGE
transverse qubits (α, j, k)	edges parallel to the z axis middle point: $(\alpha + 0.5, j, k)$
vertical qubits (i, β, k)	edges parallel to the y axis middle point: $(i, \beta + 0.5, k)$
horizontal qubits (i, j, γ)	edges parallel to the x axis middle point: $(i, j, \gamma + 0.5)$

TABLE V. Correspondence between qubits in \mathcal{C}_1 and edges of the lattice.

Points with two half-integer and one integer entries do not intersect any edge and sit in the center of a (possibly incomplete) square face. These points correspond to X -stabilisers which we therefore identify with faces. Given a triplet corresponding to one of such a point, the associated X -stabiliser has support contained in the set of edges which are parallel to the edges of the square, forming a cross in a plane. X -stabilisers, like qubits, are of three different types, being in one-to-one correspondence with basis elements of \mathcal{C}_2 . Namely, each X -stabiliser in \mathcal{C}_2 has support in two out of three type of qubits: transverse-vertical, transverse-horizontal or vertical-horizontal (see Table VI and Fig. 5c).

Points with integer coordinates are associated to Z -stabilisers; these are points where endpoints of edges intersect. The Z -stabiliser corresponding to (i, j, k) has support on a 3D cross of edges/qubits centered in $(z, y, x) = (i, j, k)$ (see Table VI and Fig. 5d).

Points with half-integer coordinates sit in the center of a cube. To any such cube is associated a metacheck in \mathcal{C}_3 . Metachecks have support on a 3D cross of faces/ X -stabilisers parallel to the faces of the cube they are associated to (see Table VI).

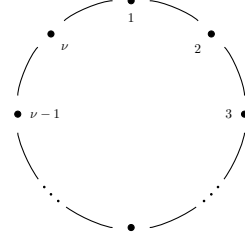
1. On geometric locality

One interesting feature of the embedding of 3D product codes on a cubic lattice is that it preserves some locality properties of the seed matrices δ_A , δ_B and δ_C . Thus, if we were able to place qubits on a 3D cubic lattice we could use the 3D homological product to build LDPC codes with nearest neighbour interactions.

Let δ be an $m \times n$ matrix with row/column indices $\alpha \in \{1, \dots, m\}$ and $i \in \{1, \dots, n\}$ respectively and let $\nu = \max\{m, n\}$. We say that δ is *geometrically ρ -local on a torus* if for any row and any column index:

$$\alpha^* \subseteq U_{\rho, \nu}(\alpha) \quad \text{and} \quad i^* \subseteq U_{\rho, \nu}(i), \quad (\text{A3})$$

where $U_{\rho, \nu}(\zeta)$ is any set of ρ consecutive integers modulo ν which contains ζ . In particular, we require the α th rows to have support on columns with index that is *close* to the integer α , and similar for columns. The reason for this choice will be clear when we prove Prop. 1. Briefly, conditions (A3) says that δ is geometrically ρ -local on a torus if: (1) any of its rows has support on a bounded box of ρ -columns, and the box for row $\alpha + 1$ is a right shift of the box for row α ; (2) any of its columns has support on a bounded box of ρ rows, and the box for column $i + 1$ is a downward shift of the box for column i . In particular, if we associate row/column indices with integer points on a circle of ν points:



locality means that any set α^*/i^* is contained in a closed interval on the circle such that (i) it has length at most ρ and (ii) it contains the point α/i . For instance, the degenerate parity check matrix of the repetition code:

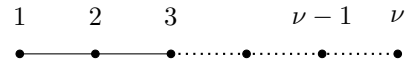
$$\begin{pmatrix} 1 & 1 & 0 & 0 & 0 \\ 0 & 1 & 1 & 0 & 0 \\ 0 & 0 & 1 & 1 & 0 \\ 0 & 0 & 0 & 1 & 1 \\ 1 & 0 & 0 & 0 & 1 \end{pmatrix}$$

is ρ -local for $\rho = 2$.

A closely related notion of locality on a torus is geometric locality in Euclidean space. We say that an $m \times n$ matrix is *geometrically ρ -local in Euclidean space* if for any row and column index:

$$\alpha^* \subseteq U_{\rho}(\alpha) \quad \text{and} \quad i^* \subseteq U_{\rho}(i), \quad (\text{A4})$$

where $U_{\rho}(\zeta)$ is any set of ρ consecutive integer in $[1, \dots, \nu]$, $\nu = \max\{m, n\}$, which contains ζ . In this case we can graphically picture locality by associating row/column indices with integer points on a line of ν points:



A matrix is local if any set α^*/i^* is contained in a closed interval on the line such that (i) it has length at most ρ and (ii) it contains the point α/i . For example, the full-rank parity check matrix of the repetition code:

$$\begin{pmatrix} 1 & 1 & 0 & 0 & 0 \\ 0 & 1 & 1 & 0 & 0 \\ 0 & 0 & 1 & 1 & 0 \end{pmatrix}$$

is 2-local.

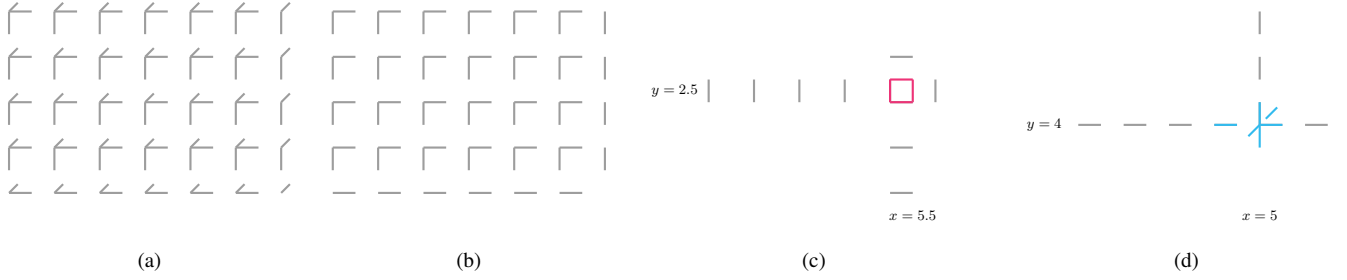


FIG. 5. Graphical representation of the cubic lattice associated to a 3D product code where the seed matrices δ_A , δ_B , δ_C have size 2×3 , 4×5 , 6×7 respectively. In (a) and (b) the lattice is depicted per slice i.e. edges of the lattice with same z -coordinate; the first and second slice of the lattice are the same (a) while the third is different (b). In (c) and (d) the support of an X -stabiliser and a Z -stabiliser highlighted. (c) The position of the X -stabiliser indexed by $(i, \beta, \gamma) = (1, 2, 5)$ is highlighted in red; its support is contained in the cross of vertical and horizontal qubits (red and grey edges) in the xy -plane $\{z = 1\}$. The crossing has coordinates $(z, y, x) = (1, 2.5, 5.5)$ and sits in the center of the red square. (d) The position of the Z -stabiliser indexed by $(i, j, k) = (1, 4, 5)$ is highlighted in blue; its support is contained in the 3D cross of qubits depicted (blue and grey edges). The crossing has coordinates $(z, y, x) = (1, 4, 5)$ and sits on the blue vertex.

OPERATOR	TYPE	SUPPORT
X -stabilisers	transverse-vertical square (α, β, k)	transverse qubits: (α, β^*, k) vertical qubits: (α^*, β, k)
	transverse-horizontal square (α, j, γ)	transverse qubits: (α, j, γ^*) horizontal qubits: (α^*, j, γ)
	vertical-horizontal square (i, β, γ)	vertical qubits: (i, β, γ^*) horizontal qubits: (i, β^*, γ)
Z -stabilisers	(i, j, k)	transverse qubits: (i^*, j, k) vertical qubits: (i, j^*, k) horizontal qubits: (i, j, k^*)
metachecks	(α, β, γ)	transverse-vertical faces: $(\alpha, \beta, \gamma^*)$ transverse-horizontal faces: $(\alpha, \beta^*, \gamma)$ vertical-horizontal faces: $(\alpha^*, \beta, \gamma)$

TABLE VI. Correspondence between operators of the chain complex \mathcal{C} , their type as geometric objects on the lattice, and their support. Note that the support of X and Z stabilizers is a set of qubits/edges while the support of metachecks is a set of X -stabilisers/faces.

Geometric locality also applies to codes other than the repetition code. For instance, the matrix

$$H = \begin{pmatrix} 1 & 1 & 0 & 0 & 0 & 0 & 0 & 0 & 0 \\ 0 & 1 & 0 & 0 & 0 & 0 & 1 & 0 & 0 \\ 0 & 0 & 1 & 1 & 0 & 0 & 0 & 0 & 0 \\ 0 & 0 & 0 & 1 & 0 & 0 & 0 & 1 & 0 \\ 0 & 0 & 0 & 0 & 1 & 1 & 0 & 0 & 0 \\ 0 & 0 & 0 & 0 & 0 & 1 & 0 & 0 & 1 \\ 1 & 0 & 1 & 0 & 1 & 0 & 0 & 0 & 0 \end{pmatrix},$$

obtained via the edge augmentation procedure presented in [47] is 7-local on a torus. We remark that geometric locality is a property of matrices. For example, the matrix with same row as H but different ordering $\{1, 2, 3, 4, 7, 5, 6\}$, is geometrically 5-local on torus.

In general, geometric locality is a relaxation of the locality property of the repetition code which only allows for interactions between pairs of nearest bits. Importantly, as Prop. 1 states, it is preserved by the 3D product construction. For this reason, geometrically local classical codes, combined with the 3D product construction, could be good candidates in the quest to quantum local codes beyond the toric and the surface codes.

The remainder of this Appendix is organised as follows.

We first state Prop. 1 and prove that geometric locality is preserved by the 3D product construction. We conclude by observing how this proof provides an explicit identification of the 3D toric and surface codes as 3D product codes.

To ease the notation, in the following we will shortly refer to codes as geometrically local, dropping the specification on a torus/in Euclidean space. When considering qubits on a cubic lattice, the lattice would be on a torus or in Euclidean space depending on the definition of locality that applies to the seed matrices.

Proposition 1. *Consider the 3D product code obtained from three seed matrices geometrically ρ -local. If its qubits are displayed on the edges of a cubic lattice as detailed in Sec. A, then it is geometrically ρ -local in the following sense:*

1. any X -stabiliser generator has weight at most 2ρ with support contained in a 2D box of size $\rho \times \rho$,
2. any Z -stabiliser generator has weight at most 3ρ with support contained in a 3D box of size $\rho \times \rho \times \rho$.

Proof. We prove the condition on the Z -stabilisers, the proof for the X -stabiliser being similar.

Let S_z be a Z -stabiliser generator. As reported in Table VI and VI, it is the image of a basis vector $(e_i^{A_0} \otimes e_j^{B_0} \otimes e_k^{C_0}) \in \mathcal{C}_0$

via the map δ_1 and it corresponds to the point on the lattice of integers coordinates (i, j, k) . By exploiting the choice of the basis for the spaces \mathcal{C}_0 and \mathcal{C}_1 and some linear algebra :

$$\begin{aligned} \delta_1(e_i^{A_0} \otimes e_j^{B_0} \otimes e_k^{C_0}) &= \sum_{\alpha \in i^*} (e_\alpha^{A_1} \otimes e_j^{B_0} \otimes e_k^{C_0}, 0, 0) \\ &+ \sum_{\beta \in j^*} (0, e_i^{A_0} \otimes e_\beta^{B_1} \otimes e_k^{C_0}, 0) \\ &+ \sum_{\gamma \in k^*} (0, 0, e_i^{A_0} \otimes e_j^{B_0} \otimes e_\gamma^{C_1}). \end{aligned}$$

Again using Table IV, the set of indices which corresponds to this sum of basis vectors of \mathcal{C}_1 can be written as:

$$\begin{aligned} \text{indices}(S_z) = & \{(\alpha, j, k) \mid \alpha \in i^*\} \\ & \cup \{(i, \beta, k) \mid \beta \in j^*\} \\ & \cup \{(i, j, \gamma) \mid \gamma \in k^*\}. \end{aligned}$$

Following the nomenclature of qubits as traversal, vertical and horizontal, we see that the three components of the support of S_z given above respect this division and therefore we can write:

$$\text{indices}(S_z) = \text{indices}(S_z)_t \cup \text{indices}(S_z)_v \cup \text{indices}(S_z)_h.$$

Using (A4) (or (A3)), we see that the sets $\text{indices}(S_z)_t$, $\text{indices}(S_z)_v$ and $\text{indices}(S_z)_h$ correspond respectively to the three sets of consecutive coordinates on the lattice:

$$\begin{aligned} \Pi_t &= \{(\bar{i}, j, k) \mid \bar{i} \in U_\rho(i)\}, \\ \Pi_v &= \{(i, \bar{j}, k) \mid \bar{j} \in U_\rho(j)\}, \\ \Pi_h &= \{(i, j, \bar{k}) \mid \bar{k} \in U_\rho(k)\}. \end{aligned}$$

Since we required $\zeta \in U_\rho(\zeta)$ (or $\zeta \in U_{\rho,\nu}(\zeta)$), the three sets of coordinates intersect on the point $(z, y, x) = (i, j, k)$. Moreover, all three intervals Π_t, Π_v, Π_h have length at most ρ . Combining these, we find that the support of S_z indexed by (i, j, k) is contained in a $\rho \times \rho \times \rho$ neighborhood of the point $(z, y, x) = (i, j, k)$ and has cardinality at most 3ρ . In other words, we have showed that the support of S_z is contained on a 3D cross of qubits with arms of length at most ρ . \square

As previously said, the 3D toric and planar codes are particular instances of the 3D product construction. Furthermore, it is well known that they are local on a torus and in the Euclidean space respectively (see Fig. 6). To see how this is the case, we remind the reader that the 3D toric code is obtained by choosing as seed matrices the degenerate parity check matrix of the repetition code in the standard basis. For matrix size $L \times L$, it holds that

$$\begin{aligned} \{1, \dots, L\} &\longleftrightarrow \{1, \dots, L\} \\ i &\longrightarrow \{i, i+1 \bmod L\} \\ \{\alpha, \alpha+1 \bmod L\} &\longleftarrow \alpha \end{aligned}$$

Therefore, stabilisers have support on pairs of consecutive edges, and it is straightforward to see that they have the usual shape:

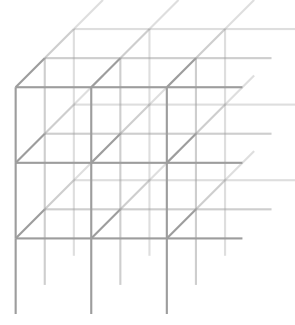


FIG. 6. Complete lattice for a symmetric case. Here the seed matrices δ_A, δ_B and δ_C have all size 3×3 .

1. Z -stabilisers have support on edges incident to a vertex;
2. X -stabilisers have support on edges on the boundary of a square face;
3. metachecks have support on the faces of a cube.

A similar argument holds for the 3D surface code, which is local in Euclidean space.

Appendix B: All 3D product codes have X-confinement

In this Section we prove Theorem 2 which states that all 3D product codes have X -confinement. Our proof follows the proof of soundness for 4D codes given in [18] with some minor adaptations and it is here reported for completeness.

First, we show that an opportunely chosen length-2 chain complex has confined maps. Secondly, we explain how to use this chain complex as a building block of the length-3 chain complex \mathcal{C} described in Sec. III. Lastly, we prove that the confinement property is preserved and thus 3D codes defined on \mathcal{C} as explained in Sec. III have X -confinement.

Let $\delta_A : C_A^0 \rightarrow C_A^1$ and $\delta_B : C_B^0 \rightarrow C_B^1$ be two length-1 chain complexes. We consider the length-2 product complex $\tilde{\mathcal{C}}$ defined as:

$$\begin{array}{ccc} & C_A^1 \otimes C_B^1 & \\ \swarrow & & \searrow \\ C_A^1 \otimes C_B^0 & & C_A^0 \otimes C_B^1 \\ \swarrow & & \searrow \\ & C_A^0 \otimes C_B^0 & \end{array} \quad \begin{array}{c} \tilde{\mathcal{C}}_2 \\ \uparrow \tilde{\delta}_1 \\ \tilde{\mathcal{C}}_1 \\ \uparrow \tilde{\delta}_0 \\ \tilde{\mathcal{C}}_0 \end{array}$$

where

$$\begin{aligned} \tilde{\delta}_0 &= (\delta_A \otimes \mathbb{1} \quad \mathbb{1} \otimes \delta_B), \\ \tilde{\delta}_1 &= \begin{pmatrix} \mathbb{1} \otimes \delta_B \\ \delta_A \otimes \mathbb{1} \end{pmatrix}; \end{aligned}$$

We first show that the map $\tilde{\delta}_0$ has confinement.

Lemma 3. $\tilde{\delta}_0$ has (t, f) -confinement where $t = \min\{d_A, d_B\}$ and $f(x) = x^2/4$.

Proof. In order to prove Lem. 3 we first introduce some useful notation. When considering vectors v in a two-fold tensor product space $\mathbb{F}^{n_1} \otimes \mathbb{F}^{n_2}$ it can be handy to consider their reshaping, which is $n_1 \times n_2$ matrix on \mathbb{F} . Namely, fixed bases $\mathcal{B}^1 = \{a_1, \dots, a_{n_1}\}$ and $\mathcal{B}^2 = \{b_1, \dots, b_{n_2}\}$ of \mathbb{F}^{n_1} and \mathbb{F}^{n_2} respectively, their product

$$\mathcal{B} = \{a_i \otimes b_j\}_{\substack{i=1, \dots, n_1 \\ j=1, \dots, n_2}}$$

is a basis of $\mathbb{F}^{n_1} \otimes \mathbb{F}^{n_2}$. Therefore, we can write

$$v = \sum_{a_i \otimes b_j \in \mathcal{B}} v_{ij} a_i \otimes b_j \quad (\text{B1})$$

for some $v_{ij} \in \mathbb{F}$. We call the matrix V whose entries are the coefficient v_{ij} the reshaping of v . Given matrices M and N of size $n_1 \times m_1$ and $n_2 \times m_2$ associated to linear maps from \mathbb{F}^{n_1} and \mathbb{F}^{n_2} respectively, the map $M \otimes N$ from $\mathbb{F}^{n_1} \otimes \mathbb{F}^{n_2}$ to $\mathbb{F}^{m_1} \otimes \mathbb{F}^{m_2}$ acts on the reshaping of v as:

$$(M \otimes N)V \longmapsto MVN^T. \quad (\text{B2})$$

In the following we will always indicate with lower-case symbol vectors and with the corresponding upper-case symbols their reshaping. We can now use this notation to prove Lem. 3. Let $v \in C_0^A \otimes C_0^B$ and let $s = \check{\delta}_0(v)$. By reshaping,

$$S = \begin{pmatrix} \delta_A V \\ V \delta_B^T \end{pmatrix}.$$

If we assume $|v| \leq t = \min\{d_A, d_B\}$ then V has no column in $\ker \delta_A$ and no row in $\ker \delta_B^T$ so that

$$\text{col}(\delta_A V) = \text{col}(V) \text{ and } \text{row}(V \delta_B^T) = \text{row}(V),$$

where $\text{col}(V)/\text{row}(V)$ is the number of non-zero columns/rows of the matrix V . Therefore, for the weight of S , it holds that:

$$\begin{aligned} |S| &= |\delta_A V| + |V \delta_B^T| \geq \text{col}(\delta_A V) + \text{row}(V \delta_B^T) \\ &= \text{col}(V) + \text{row}(V). \end{aligned}$$

Combining this with $(a+b)^2/4 \geq ab$ for integers a, b yields:

$$|S|^2/4 \geq \text{col}(V) \cdot \text{row}(V) \geq |V|. \quad \square$$

We want to use Lemma 3 to infer that the code defined on the chain complex \mathcal{C} has X -confinement. To see how this is the case, we consider an ‘asymmetrical’ version of \mathcal{C} as the product of the length-2 chain complex $\tilde{\mathcal{C}}$ and the length-1 chain complex $\delta_C : C_0^C \rightarrow C_1^C$. The asymmetric product complex $\check{\mathcal{C}}$ is then

$$\begin{array}{ccccc} & & \tilde{\mathcal{C}}_2 \otimes C_C^1 & & \check{\mathcal{C}}_3 \\ & \nearrow & & \nwarrow & \uparrow \check{\delta}_2 \\ \tilde{\mathcal{C}}_1 \otimes C_C^1 & & & & \check{\mathcal{C}}_2 \\ & \nwarrow & & \nearrow & \uparrow \check{\delta}_1 \\ \tilde{\mathcal{C}}_0 \otimes C_C^1 & & \tilde{\mathcal{C}}_2 \otimes C_0^C & & \check{\mathcal{C}}_1 \\ & \nwarrow & & \nearrow & \uparrow \check{\delta}_0 \\ & & \tilde{\mathcal{C}}_0 \otimes C_0^C & & \check{\mathcal{C}}_0 \end{array}$$

where

$$\check{\delta}_0 = \begin{pmatrix} \mathbb{1} \otimes \delta_C \\ \check{\delta}_0 \otimes \mathbb{1} \end{pmatrix},$$

$$\check{\delta}_1 = \begin{pmatrix} \check{\delta}_0 \otimes \mathbb{1} & \mathbb{1} \otimes \delta_C \\ 0 & \check{\delta}_1 \otimes \mathbb{1} \end{pmatrix},$$

$$\check{\delta}_2 = (\check{\delta}_1 \otimes \mathbb{1} \quad \mathbb{1} \otimes \delta_C).$$

Claim 1. Let $(v, w) \in \check{\mathcal{C}}_1$ have weight less than t and $s = \check{\delta}_1(v, w)$ be its syndrome. If (V, W) is the reshaping of the vector (v, w) then the following Syndrome Equation holds:

$$S = \begin{pmatrix} S_1 \\ S_2 \end{pmatrix} = \begin{pmatrix} \check{\delta}_0 V + W \delta_C^T \\ \check{\delta}_1 W \end{pmatrix}, \quad (\text{SE})$$

where S is the reshaping of s .

Note that a stabiliser for the chain complex $\check{\mathcal{C}}_0 \rightarrow \check{\mathcal{C}}_1 \rightarrow \check{\mathcal{C}}_2 \rightarrow \check{\mathcal{C}}_3$ and the syndrome map $\check{\delta}_1(\cdot)$ has the form $\check{\delta}_0(m)$ for some $m \in \check{\mathcal{C}}_0$. By construction, we can add any stabiliser to (v, w) without violating the Syndrome Equation (SE). In particular,

1. $|(v, w)| < t$ entails that its reshaping satisfies the following properties:

- (a) Both V and W have at most t non-zero rows. Thus all their columns have weight at most t .
- (b) Both V and W has at most t non-zero columns. Thus all their rows have weight at most t .

2. Fix a row index i and a column index j . Let M be a matrix in $\check{\mathcal{C}}_0$ with columns

$$M^h = \begin{cases} V^j & \text{for } h \text{ in } \text{supp}(W \delta_C^T)_i = \text{supp}(W_i \delta_C^T), \\ 0 & \text{elsewhere.} \end{cases}$$

Its image $(M \delta_C^T, \check{\delta}_0 M)$ through $\check{\delta}_0$ is a stabiliser. Define V^* and W^* as

$$V^* = V + M \delta_C^T \quad \text{and} \quad W^* = W + \check{\delta}_0 M.$$

Observe that:

(a) M is a matrix whose non-zero columns are equal to a column of V . Therefore M has row support contained in the row support of V :

$$\text{row}(V^*) \subseteq \text{row}(V). \quad (\text{B3})$$

(b) M is a matrix whose column support is $\text{supp}(W_i \delta_C^T)$ for some row W_i of W . Therefore M has column support contained in the column support of W :

$$\text{col}(W^*) \subseteq \text{col}(W). \quad (\text{B4})$$

Lemma 4 (Inheritance of confinement). $\check{\delta}_1$ has (t, f) -confinement where $t = \min\{d_A, d_B, d_C\}$ and $f(x) = \frac{x^3}{2}$.

Proof. Let $(v, w) \in \check{C}_1$ have weight less than t and $s = \check{\delta}_1(v, w)$ be its syndrome. Reshaping vectors into matrices (see Eq. (B1) and (B2)) yields the following Syndrome Equation:

$$S = \begin{pmatrix} S_1 \\ S_2 \end{pmatrix} = \begin{pmatrix} \check{\delta}_0 V + W \delta_C^T \\ \check{\delta}_1 W \end{pmatrix} \quad (\text{SE})$$

We will transform the vector (V, W) by adding stabilisers to it in order to change its column and row support. We do this by iterating the following two steps.

Step 1: Let i, j be row and column indices s.t.

- (a) $(W \delta_C^T)_i \neq 0$ and $(S_1)_i = 0$;
- (b) $(\check{\delta}_0 V)_{ij} \neq 0$ and $(W \delta_C^T)_{ij} = 1$.

Build a matrix M as in Claim 1. Transform V and W accordingly:

$$\begin{aligned} V &\mapsto V + M \delta_C^T \\ W &\mapsto W + \check{\delta}_0 M \end{aligned}$$

Note that in this way we are able to delete row i of $W \delta_C^T$.

Iterate this step till we obtain:

$$\text{row}(W \delta_C^T) \subseteq \text{row}(S_1). \quad (\text{B5})$$

Step 2: Let i, j be row and column indices s.t.

- (a) $(W \delta_C^T)^j \neq 0$ and $(S_1)^j = 0$; this entails $(\check{\delta}_0 V)^j = (W \delta_C^T)^j$;
- (b) $(\check{\delta}_0 V)_{ij} = (W \delta_C^T)_{ij} = 1$.

Build a matrix M as in Claim 1. Transform V and W accordingly:

$$\begin{aligned} V &\mapsto V + M \delta_C^T \\ W &\mapsto W + \check{\delta}_0 M \end{aligned}$$

Note that in this way we are able to delete row i of $W \delta_C^T$ and by repeatedly doing so we can delete any column j

of $W(\delta_C^T)$ which does not belongs to the column support of S_1 .

Iterate this step till we obtain:

$$\text{col}(W \delta_C^T) \subseteq \text{col}(S_1). \quad (\text{B6})$$

Let \mathbf{M} be the matrix formed by summing over all the matrices M found during these two steps. Define V^* and W^* as

$$V^* = V + \mathbf{M} \delta_C^T \quad \text{and} \quad W^* = W + \check{\delta}_0 \mathbf{M}. \quad (\text{B7})$$

We now proceed to prove an upper bound for the weight of W^* first and then one for the weight of V^* . By combining these two bounds we obtain the desired confinement relation between the weight of the syndrome and the weight of the error.

BOUND ON THE WEIGHT OF W^*

1. By Claim 1, no row of W^* has weight more than t and therefore none of them belongs to $\ker \delta_C^T$ so that $\text{row}(W^* \delta_C^T) = \text{row}(W^*)$. Combining this with Equation (B5) yields:

$$\text{row}(W^*) \subseteq \text{row}(S_1). \quad (\text{B8})$$

2. By Claim 1, the column support of W^* is contained in the column support of W which is equal to the column support of S_2 , by assumption on its weight. Summing these up:

$$\text{col}(W^*) \subseteq \text{col}(S_2). \quad (\text{B9})$$

3. Combining (B8) and (B9) yields:

$$|S_1| |S_2| \geq |W^*|. \quad (\text{B10})$$

BOUND ON THE WEIGHT OF V^* .

1. By rearranging the Syndrome Equation (SE), we can write $\check{\delta}_0 V^* = S_1 + W^* \delta_C^T$. Equations (B5) and (B6) therefore entail

$$\text{row}(\check{\delta}_0 V^*) \subseteq \text{row}(S_1), \quad (\text{B11})$$

and

$$\text{col}(\check{\delta}_0 V^*) \subseteq \text{col}(S_1). \quad (\text{B12})$$

2. By Claim 1, the row support of V^* is contained in the row support of V which has cardinality at most t . In particular, all the columns of V^* have weight at most t and therefore we can use the confinement property of the map $\check{\delta}_0$ column wise (see Lemma 3). In other words, for each column j of V^* , the following holds:

$$\frac{|(\check{\delta}_0 V^*)^j|^2}{4} \geq |(V^*)^j|. \quad (\text{B13})$$

Combining this with Equation (B11) yields:

$$\frac{|\text{row}(S_1)|^2}{4} \geq |(V^*)^j|. \quad (\text{B14})$$

3. By Claim 1, no column of V^* has weight more than t and therefore none of them belongs to $\ker \tilde{\delta}_0$ so that $\text{col}(V^*) = \text{col}(\tilde{\delta}_0 V^*)$. By Equation (B12) this entails

$$\text{col}(V^*) \subseteq \text{col}(S_1). \quad (\text{B15})$$

In other words, V^* has at most $|\text{col}(S_1)|$ non-zero columns and combining this with Equation (B14) yields:

$$\frac{|\text{row}(S_1)|^2}{4} |\text{col}(S_1)| \geq |V^*|, \quad (\text{B16})$$

which entails:

$$\frac{1}{4} |S_1|^3 \geq |V^*|. \quad (\text{B17})$$

Since $|S| = |S_1| + |S_2|$ and $|(V, W)| = |V| + |W|$, we can add the bounds found for V^* and W^* . Observing that $(a + b)^3 \geq (a^3 + a^2b + ab)$ for integer a, b , we obtain that (v^*, w^*) is a vector equivalent to (v, w) (i.e. it satisfies the Syndrome Equation (SE)) for which it holds:

$$\frac{1}{4} |s|^3 \geq |(v^*, w^*)|. \quad (\text{B18})$$

In conclusion, since $|(v^*, w^*)| \geq |(v, w)|_{\text{red}}$, we have proved that $\tilde{\delta}_1$ has confinement with respect to the function $f(x) = x^3/2$. \square

Appendix C: Fitting details

To obtain our threshold estimates, we use the standard critical exponent method [49]. Specifically, in the vicinity of the

threshold, we fit our data to the following ansatz

$$a_0 + a_1 x + a_2 x^2, \quad (\text{C1})$$

where the rescaled variable $x = (p - p_{\text{th}})L^{1/\mu}$. Examples of this fit are shown in Fig. 7.

We use the fitting method described in [12] to understand the behaviour of the 3D toric code logical error rate for error rates p significantly below threshold. Recall from Section V that we use the following ansatz:

$$p_{\text{fail}}(L) \propto (p/p_{\text{th}})^{\alpha L^\beta}, \quad (\text{C2})$$

we take the logarithm of both sides to obtain

$$\log p_{\text{fail}} = \log f(L) + \alpha L^\beta \log(p/p_{\text{th}}). \quad (\text{C3})$$

For different values of L , we plot $\log p_{\text{fail}}$ as a function of $\log(p/p_{\text{th}})$ and fit to a straight line to obtain gradients

$$g(L) = \frac{\partial \log p_{\text{fail}}}{\partial u} = \alpha L^\beta, \quad (\text{C4})$$

where $u = \log(p/p_{\text{th}})$. Finally, take the logarithm of both sides of the above to give

$$\log g = \log \alpha + \beta \log L. \quad (\text{C5})$$

We then plot $\log g$ as a function of $\log L$ and fit to a straight line to get α and β . Figure 8 illustrates the above fitting procedure for code-capacity noise (no measurement errors) and for eight rounds of single-shot error correction.

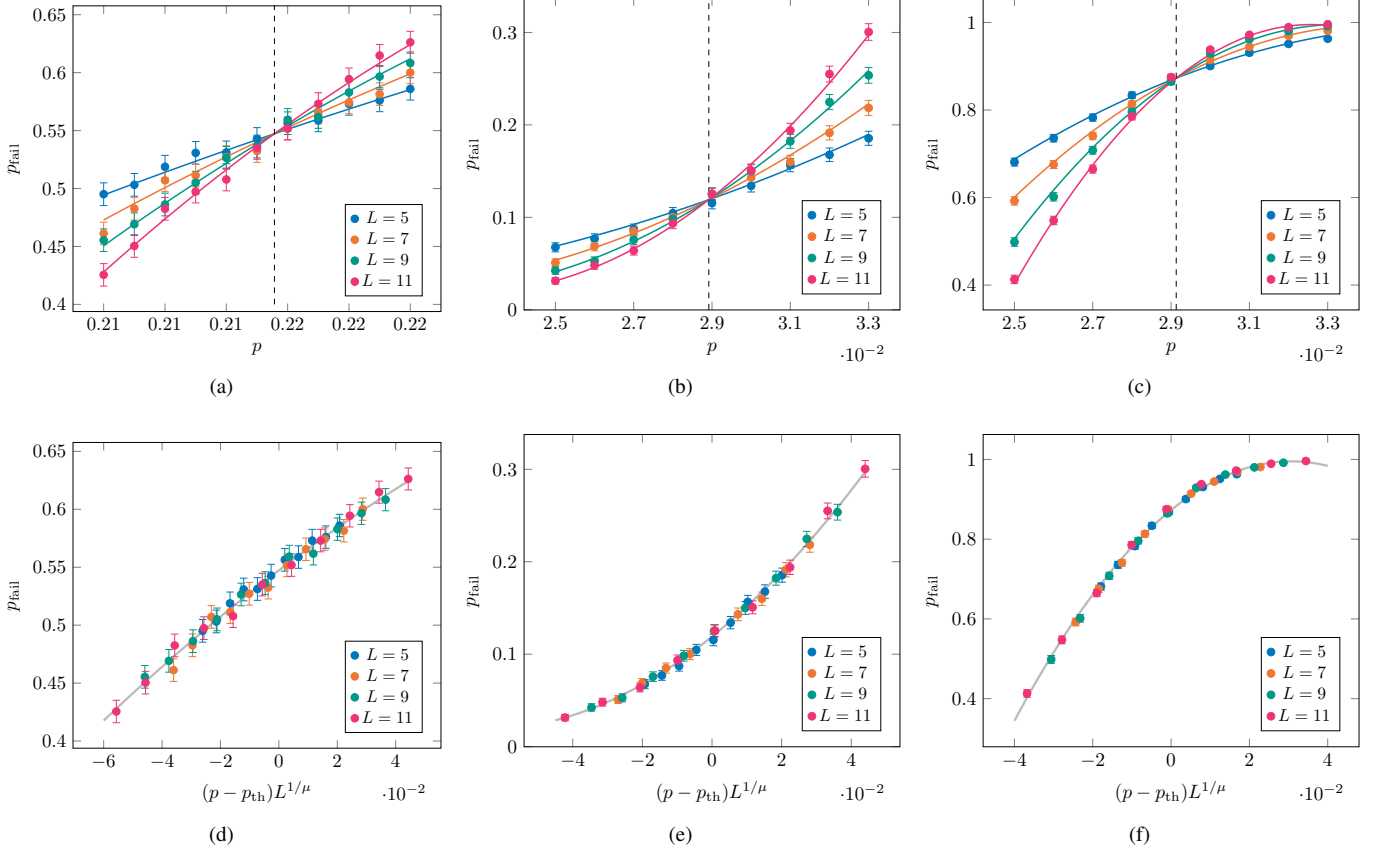


FIG. 7. Threshold fits for the 3D toric code using MWPM & BP+OSD to decode. In (a), we plot the logical error rate p_{fail} as a function of the phase-flip error rate p , for values of p close to the threshold. The coloured lines show the fit given by Eq. (C1), with parameters $a_0 = 0.547$, $a_1 = 1.92$, $a_2 = -4.04$, $\mu = 1.04$, and $p_{\text{th}} = 0.216$ (dashed grey line). In (d), we show the same data using the rescaled variable $x = (p - p_{\text{th}})L^{1/\mu}$. Subfigures (b) and (e) show equivalent data for one round of single-shot error correction, with fit parameters $a_0 = 0.119$, $a_1 = 3.04$, $a_2 = 22.9$, $\mu = 1.01$, and $p_{\text{th}} = 0.0289$. Subfigures (c) and (f) show equivalent data for sixteen rounds of single-shot error correction, with fit parameters $a_0 = 0.873$, $a_1 = 7.99$, $a_2 = -130$, $\mu = 1.10$, and $p_{\text{th}} = 0.0291$. The error bars show the 95% confidence intervals $p_{\text{fail}} = \hat{p}_{\text{fail}} \pm 1.96\sqrt{p_{\text{fail}}(1 - p_{\text{fail}})/\eta}$, where $\eta \geq 10^4$ is the number of Monte Carlo trials.

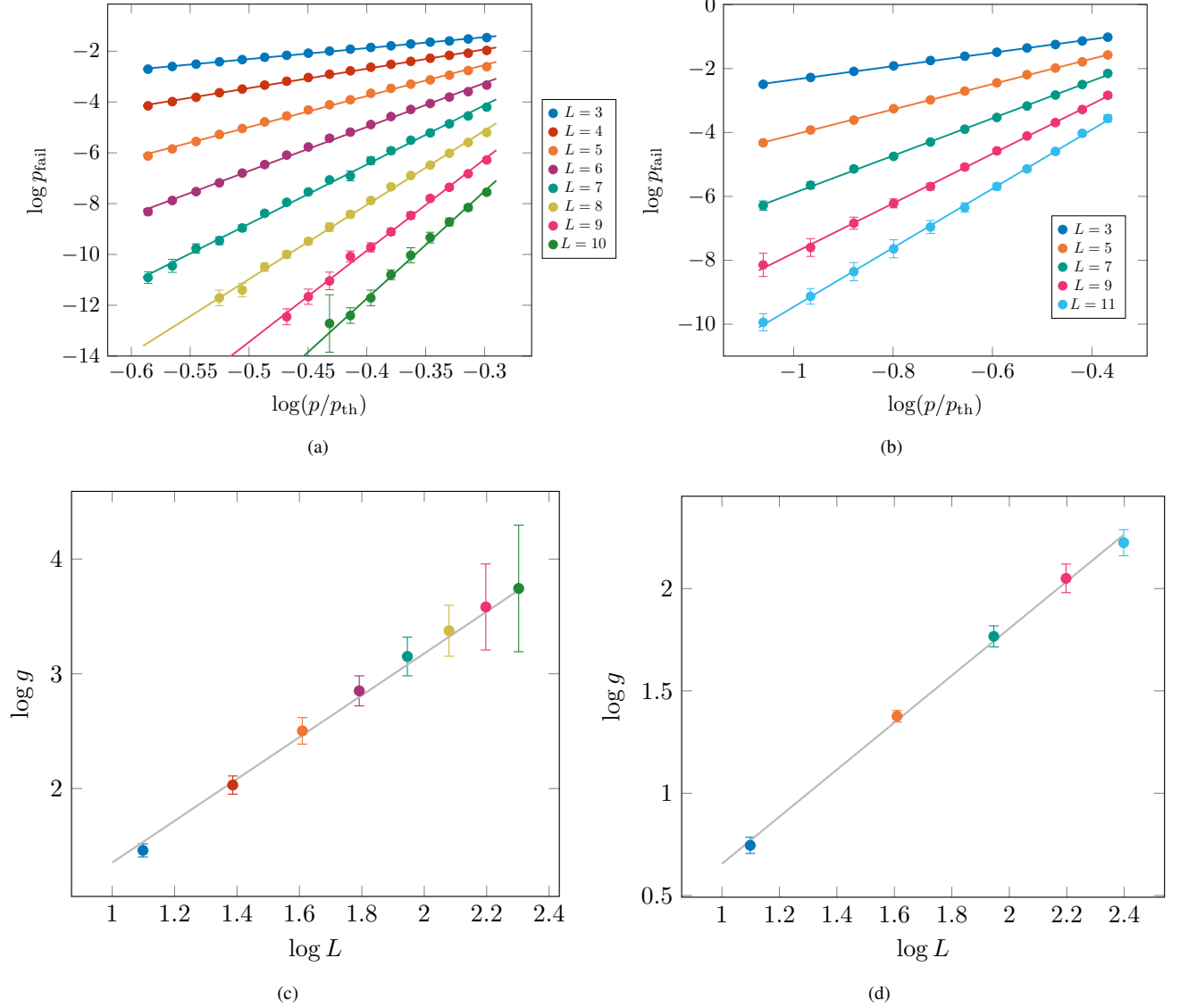


FIG. 8. Illustration of the fitting procedure for finding the coefficients describing the suppression of the logical error rate for phase-flip error rates substantially below threshold. (a) and (c) show data for code capacity noise (no measurement errors), and (b) and (d) show data for eight rounds of single-shot error correction. In both cases, we first plot $\log p_{\text{fail}}$ as a function of $\log(p/p_{\text{th}})$ for differing values of L , observing trends that agree with the straight line prediction of Eq. (C3) [(a) and (b)]. We note that for the single-shot case there is an odd-even effect so we only include the data for odd L . We extract the gradients $g(L)$ from the corresponding straight line fits in (a) and (b) (grey lines), and plot the logarithms of these values against $\log L$ [(c) and (d)]. The data fit well to the linear ansatz given in Eq. (C5), which allows us to estimate the parameters α and β , which control the suppression of the logical error rate as per Eq. (C2). For code capacity noise, we estimate $\alpha = 0.546(33)$ and $\beta = 1.91(3)$, and for eight rounds of single-shot error correction, we estimate $\alpha = 0.610(37)$ and $\beta = 1.15(3)$. The error bars in (a) and (b) show the 95% confidence intervals $\log p_{\text{fail}} = \log \hat{p}_{\text{fail}} \pm \frac{1.96}{p_{\text{fail}}} \sqrt{p_{\text{fail}}(1 - p_{\text{fail}})/\eta}$, where $\eta \geq 10^4$ is the number of Monte Carlo trials. We only include data points with at least 25 failures. The error bars in (c) and (d) show the 95% confidence intervals given by the LINEARMODELFIT function of Mathematica.